500m級超高精度レーザー直尺を用いた微小地面変動の連続観測技術の開発

T. Suwada, Y. Enomoto, K. Kakihara, K. Mikawa, T. Higo,
Accelerator Laboratory, KEK, Tsukuba, Japan

Introduction

- 超高精度レーザーアライメントシステムを利用して入射器トンネル床面の微小変動の連続観測を平成28年1月7日から開始.
- ±0.08μradの範囲内に安定化された500m級の超高精度レーザー直尺とトンネル床面に分散配置した光センサーの自動計測技術を独自に開発.
- 約半年に及ぶ観測データによると
  - 床面は決して不動ではなく、日々の動きは複雑で不規則ながらも全体的には一日当り約5μmの大きさでほぼ一様に変位していることを観測.
  - 一日当りの変位の大きさは髪毛1本の太さと比べても極めて微小で500m級超高精度レーザー直尺による計測で実現.
- スーパーBファクトリー計画(SKEKB)における入射器の性能向上に貢献するのみならず、次世代の長距離線形加速器における高精度アライメントへの応用や高度なビーム制御技術に大きく貢献すると期待.

Alignment measurement scheme for girders and components

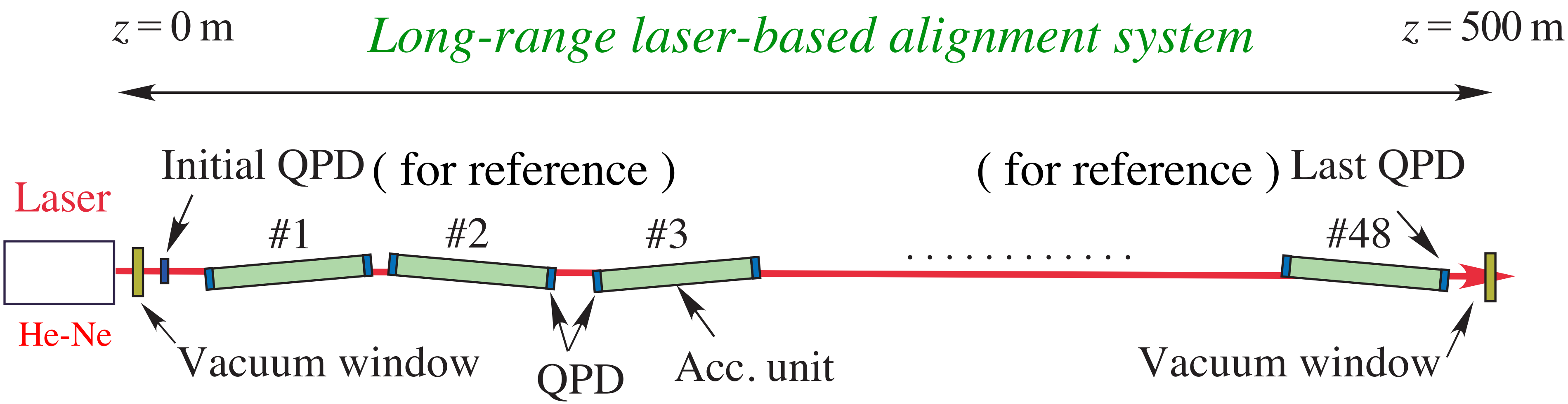

- *Long-range alignment system for girders* (accuracy σ ~ 100μm)
  The girder units can be aligned with a laser-based alignment system.
- *Short-range alignment system for components* (accuracy σ ~ 50μm)
  The accelerator components on a girder unit are aligned with a standard laser-tracker technique.

【解禁日時】平成 25 年 9 月 17 日（火）午前 1 時 （日本時間）
【本件リリース先】（資料配布）
文部科学記者会、科学記者会、筑波研究学園都市記者会

平成 25 年 9 月 13 日

報道関係者各位

大学共同利用機関法人 高エネルギー加速器研究機構

高精度アライメント※1のための長基線レーザーによる 500 m級直尺の実用化に成功

本研究成果のポイント

○市販の部品によって構成された簡便なレーザー装置を用い、これまで達成が困難であった長距離（500 m）における、加速装置を高精度で一直線上に設置する技術（高精度アライメント技術）を世界で初めて実現

○高精度アライメント技術の実現により、KEKB 加速器の高度化※2に必要とされる、安定した電子、陽電子ビームの入射が可能に

○今後の長距離線形加速器への応用のみならず、ダム事業、トンネル構築、堤防建設など、高精度な長基線を必要とする大規模土木事業などの産業応用にも大きく貢献するものと期待

Girder unit structure

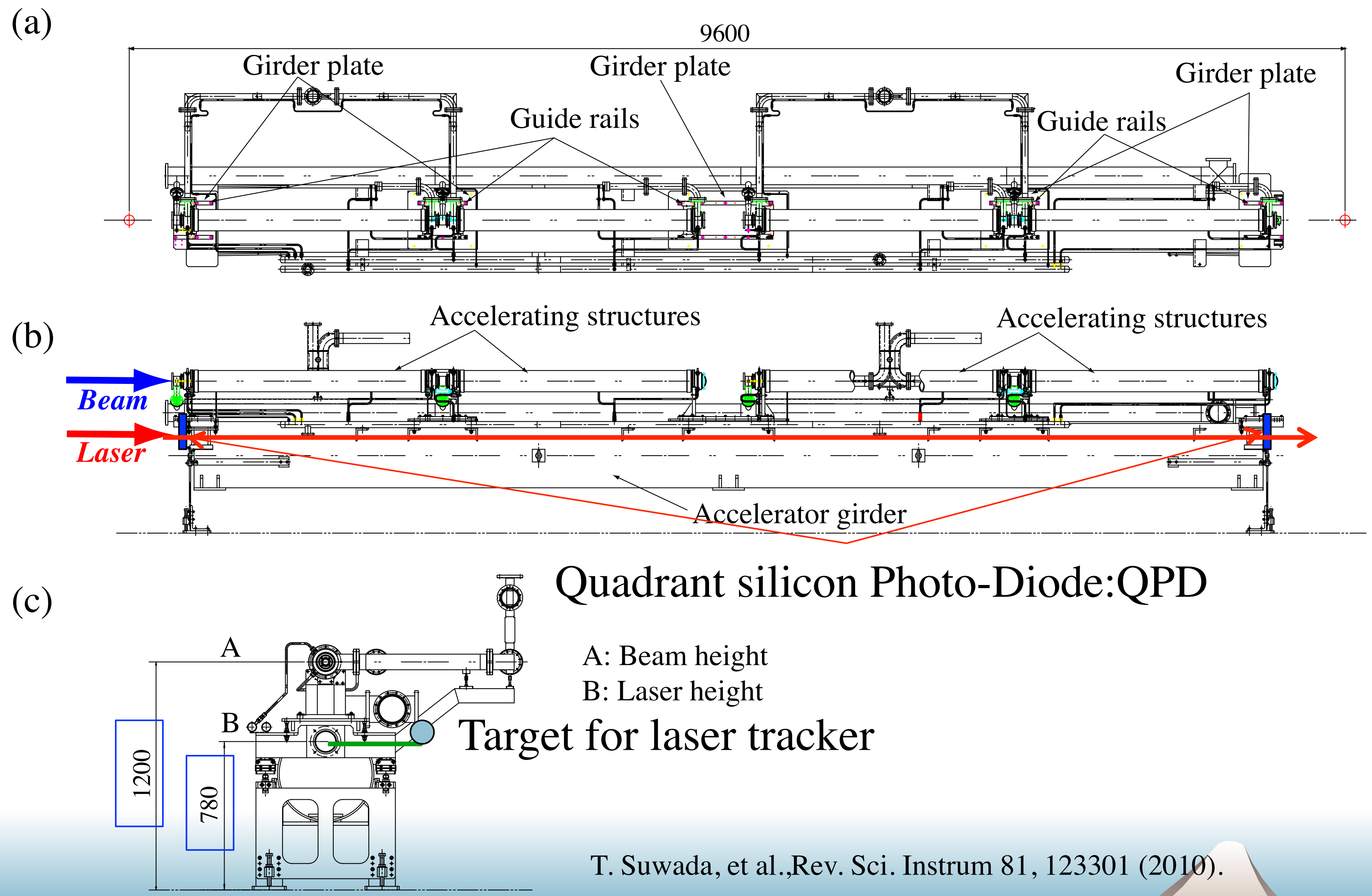

T. Suwada, et al.,Rev. Sci. Instrum 81, 123301 (2010).

KEKB linac layout and the laser-based alignment system

- Two long straight sections, AB (125m) and C5 (475m) sections with independent laser sources (He-Ne) and quadrant silicon photodiodes (QPDs).
- Two (seven) remote-controllable QPDs were installed in the summer shutdown of 2014 (2015) at multiple locations just near expansion joints (*e.j.*) of the linac building (see Table 1).

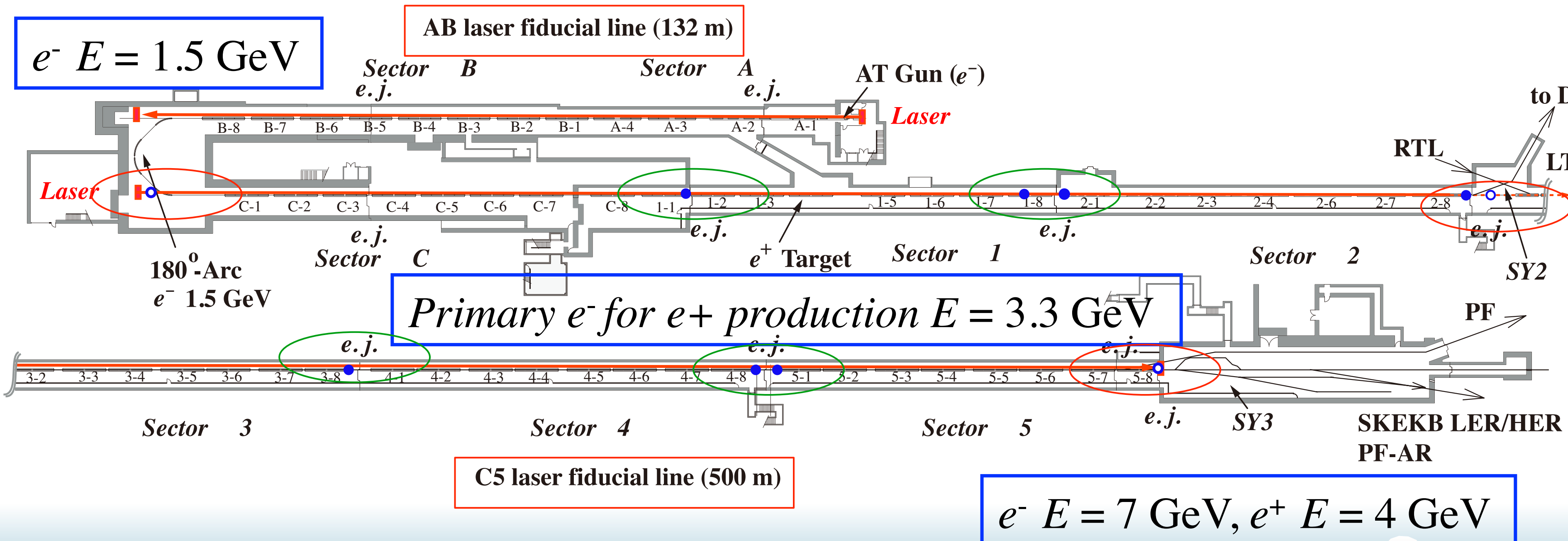

M. Akemoto, et al., Prog. Theor. Exp. Phys. 2013 , 03A002.

Table of new remote-controllable QPDs

QPD	e.j.	L [m]	r_m [mm]	s_r [μm/day]
REF1UA		1.74	0.19	3.3
	C3D	44.31	–	–
11DA		106.11	0.55	5.5
	11D	106.72	–	–
1814DA		177.04	0.65	5.1
	1814D	178.39	–	–
21UA		180.17	0.47	4.2
28G6DA		259.07	0.65	6.6
	28G6D	259.64	–	–
28REFUA		263.32	0.44	4.1
38DA		339.58	0.68	4.1
	38G5U	341.60	–	–
48DA		419.08	0.88	4.6
	48G5U	421.11	–	–
51UA		423.65	0.84	5.1
	57G7U	498.01	–	–
584D		499.94	–	–

(fixed reference QPD)

1. Summary table in the locations of the remote controllable QPDs, and expansion joints (*e.j.*) along the injector linac from the laser source.
2. Some measurement results, the maximum norm (r_m) of the displacement vector and the maximum slope (s_r) in the variations in the time traces of the norm, are also summarized depending on the QPD locations.

reference QPDs

Injection Optical System

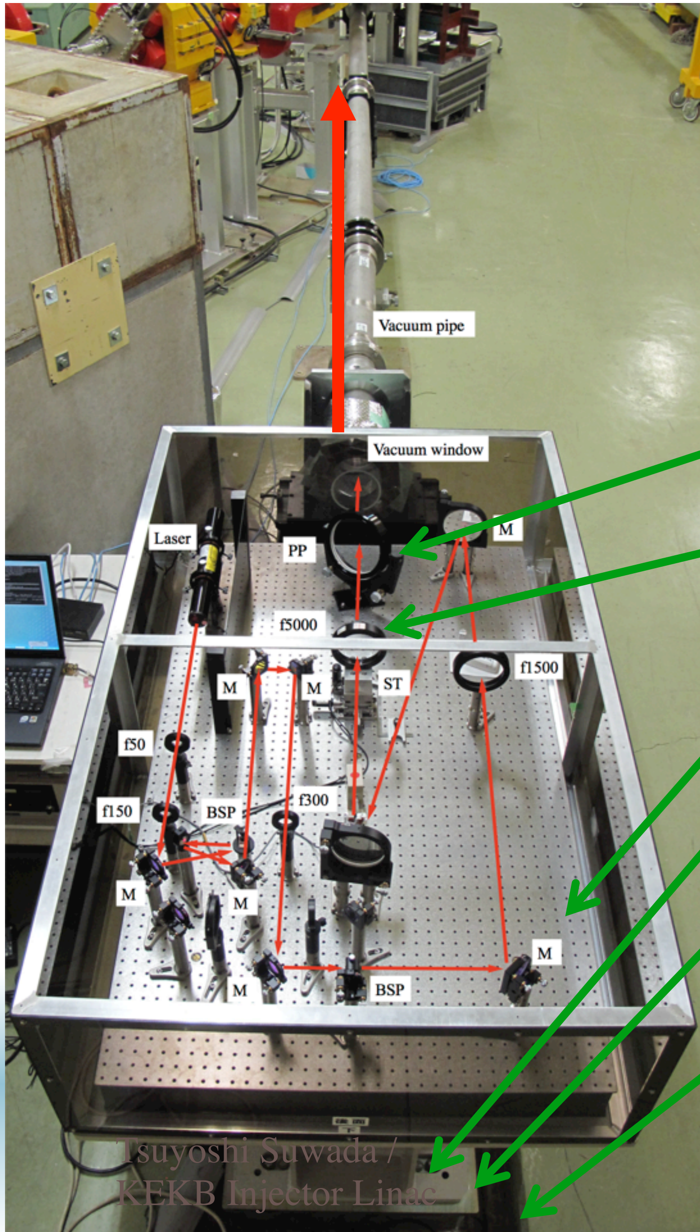

Optical system

- 10-mW He-Ne laser
- Solid and large optical table

Vacuum system

- Two scroll pumps (1000*l*/min)
- Vacuum level ~3 [Pa]

Parallel plate for translation tuning

f5000 lens for injection angle tuning

Optical table (1500×900×112^{t}mm^{3})

Girder (Fe)

Iron plate (1510×500×20^{t}mm^{3})

Isolated floor separated from the tunnel floor by a 100-mm gap (1510×500mm^{2})

Laser optical system – simple dioptric system using dioptric lenses and reflecting mirrors –

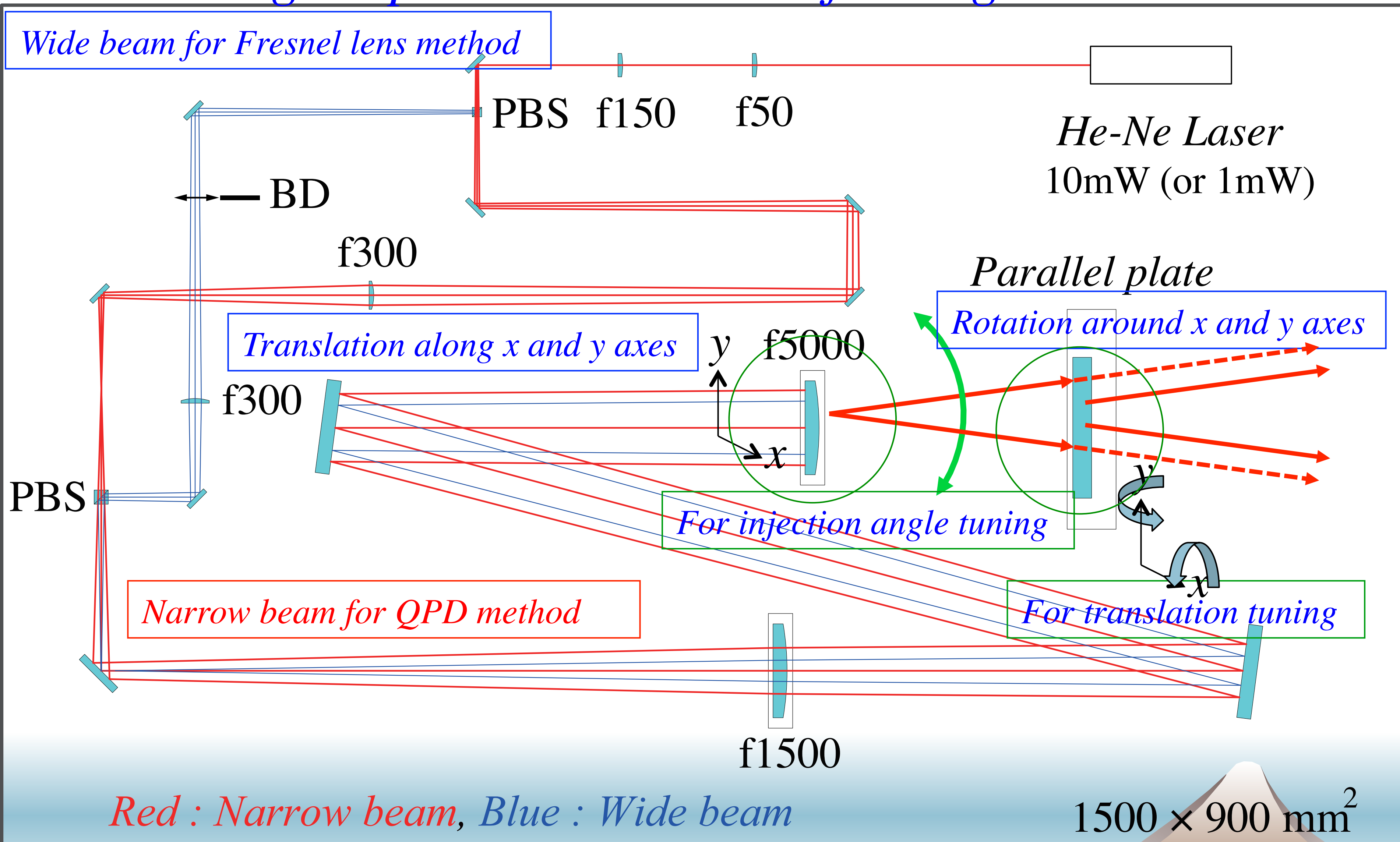

Laser profiles at the initial and last QPDs

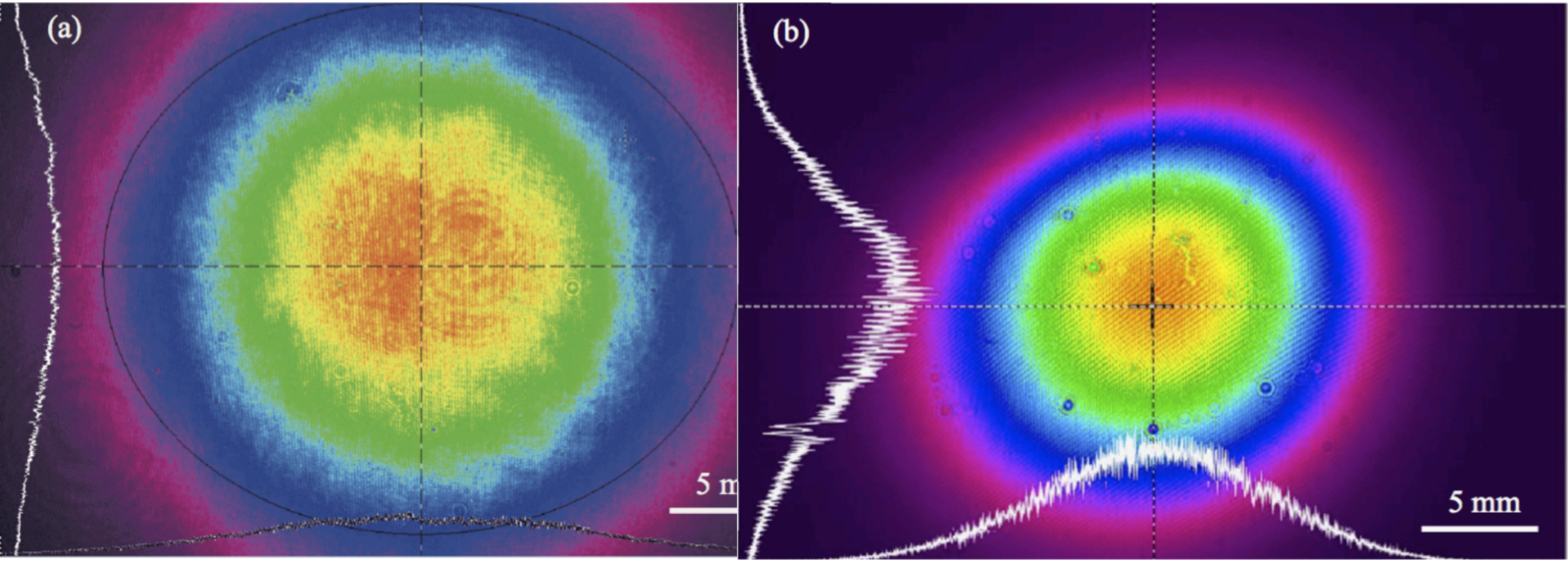

@ Exit of the optical system (z=0)
$Wx \approx Wy \approx$ 29mm (4σ width)

@ Last QPD (z=500m)
$Wx \approx$ 21.2mm(4σ width)
$Wy \approx$ 17.8mm

Sensitivity measurements of the laser axis at z = 500m

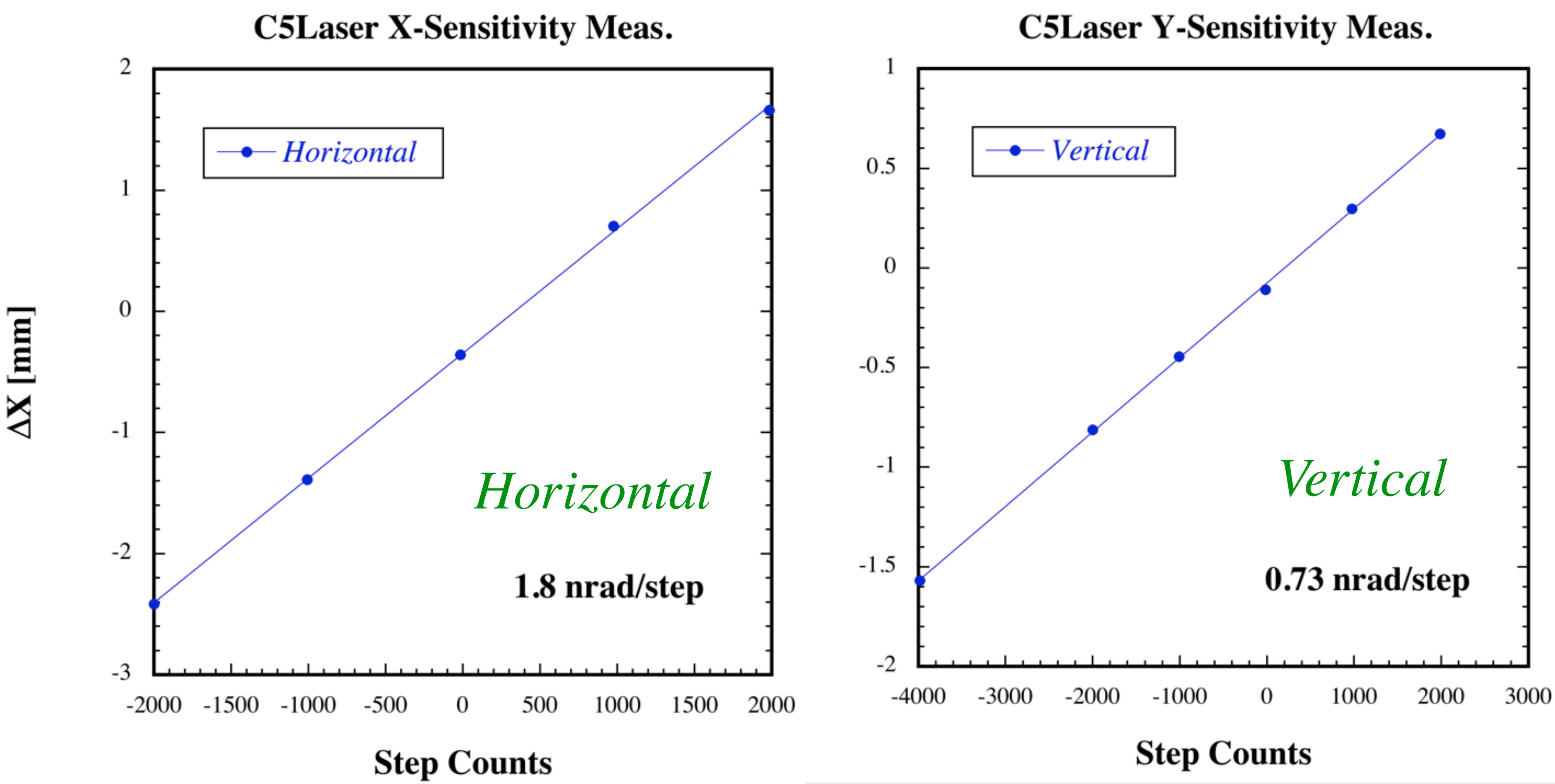

Feedback control for stabilizing an injection laser axis

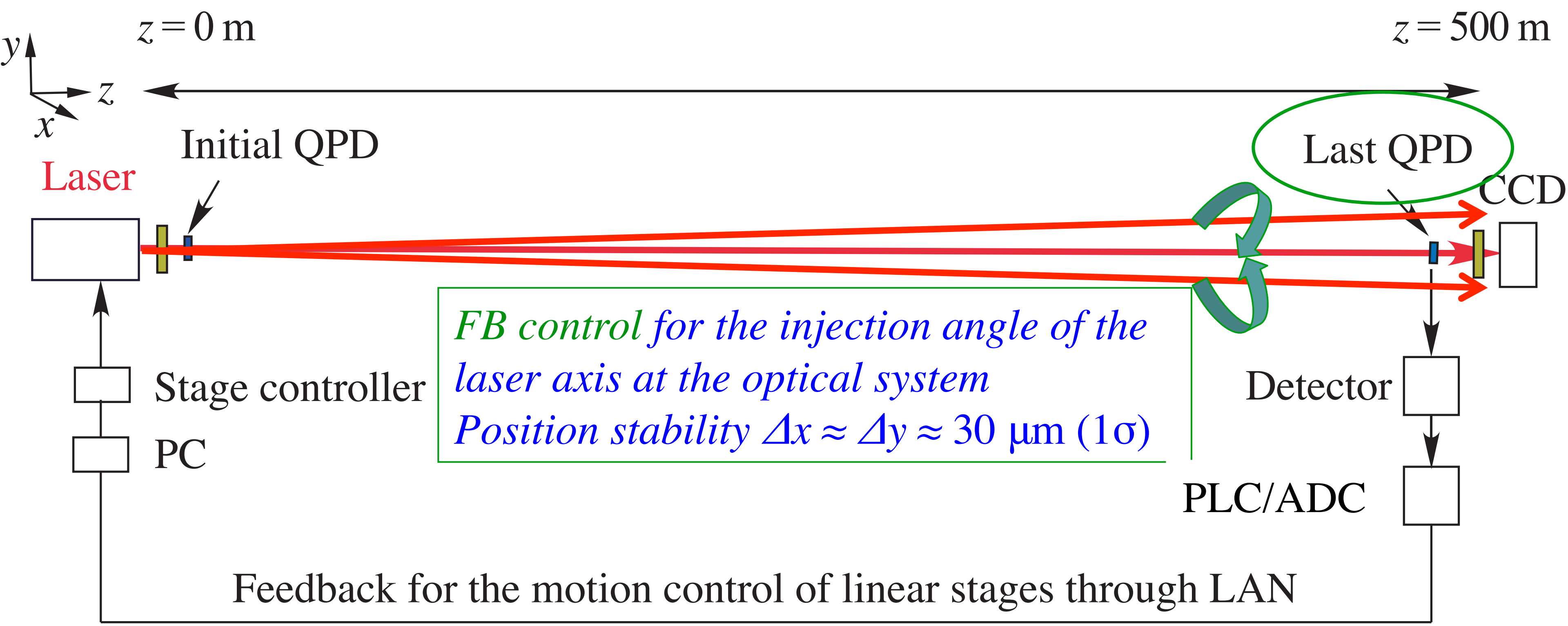

Stage with pico-motors for f5000 lens (Crucial for stable laser axis)

- M-562-XYZ/Newport, translational resolution 30nm/step → ~1nrad/step
- The drive shaft is rotated by frictional force of piezoelectric element and the stage translates in the transverse plane.

Position stability of the laser axes at the last QPD (z=500m)

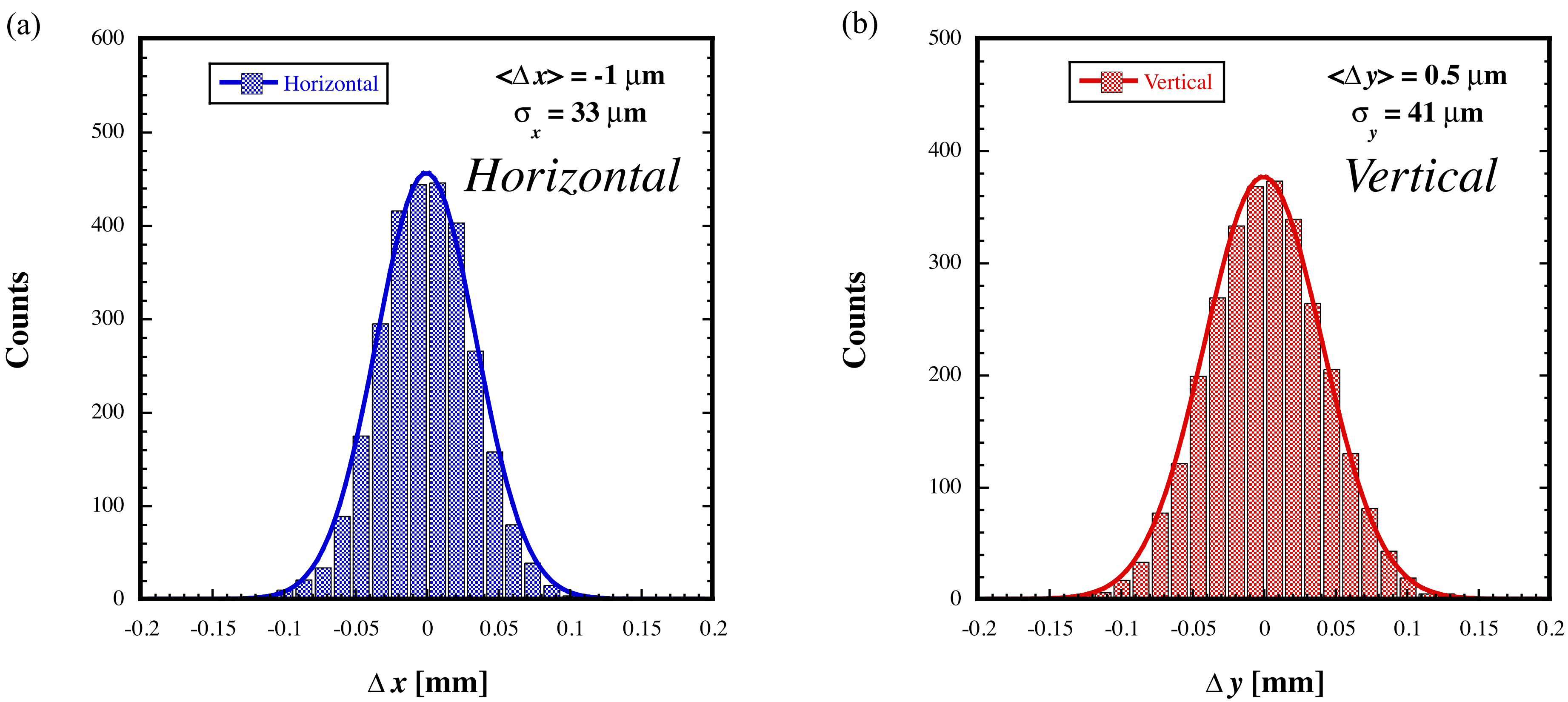

Calibration procedure for the QPD displacement to the laser axis

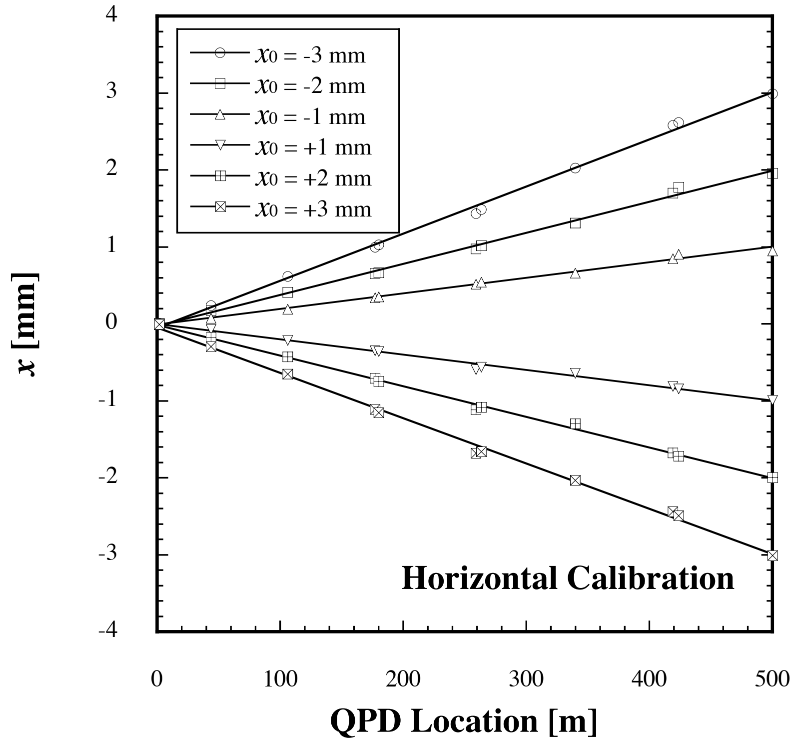

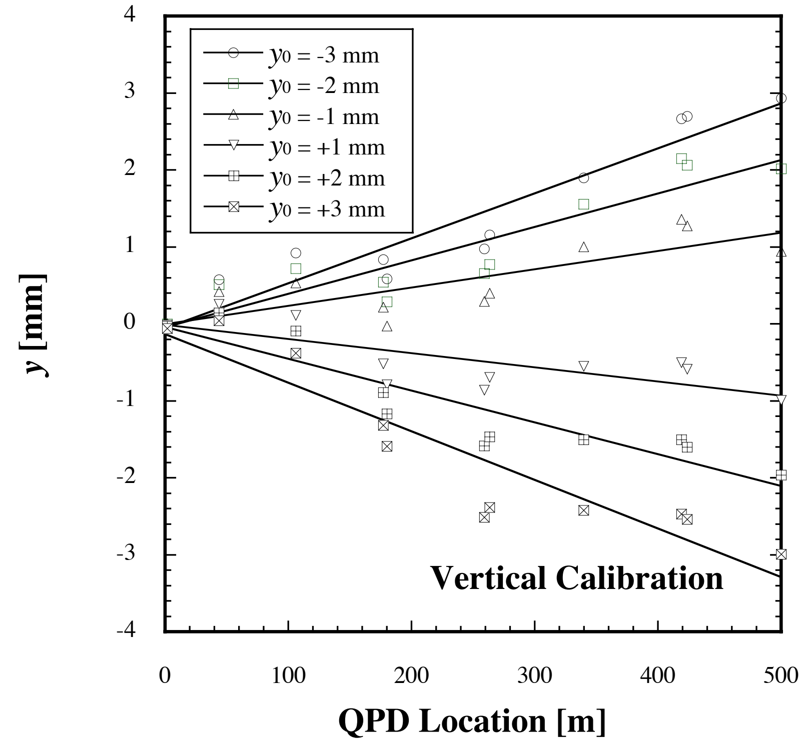

- Results in the horizontal calibration procedure for all the remote-controllable QPDs. It should be noted that a laser source and the fiducial QPDs are located at z = 0 and z = 500 m, respectively. The target positions controlled with the feedback control are defined by x_0 and y_0 at z = 500 m.

Remote-Controllable Quadrant Silicon Photodiode (QPD)

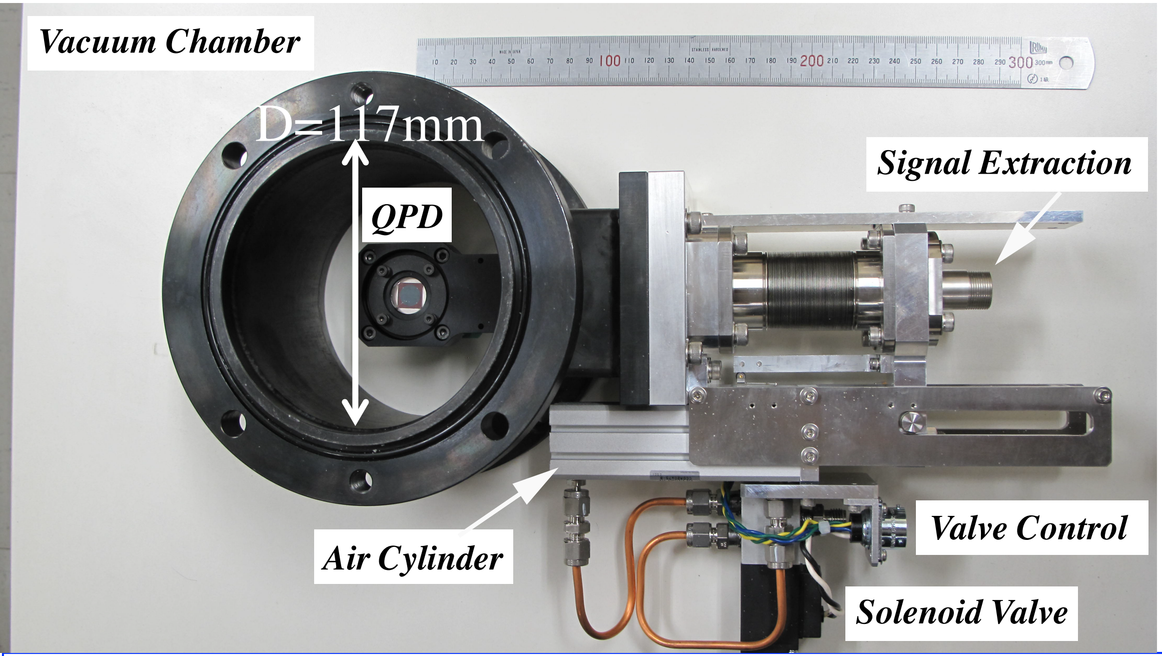

- A remote-controllable QPD sensor, QPD: OSI Optoelectronics, SPOT-9D (D =10mmϕ)
- Aperture D = 117 mm (effect. aperture D = 92 mm)
- Actuator-based QPD driving system with a compact air cylinder and a micro-solenoid valve driven by a compressed air

Detector circuit in the local control system

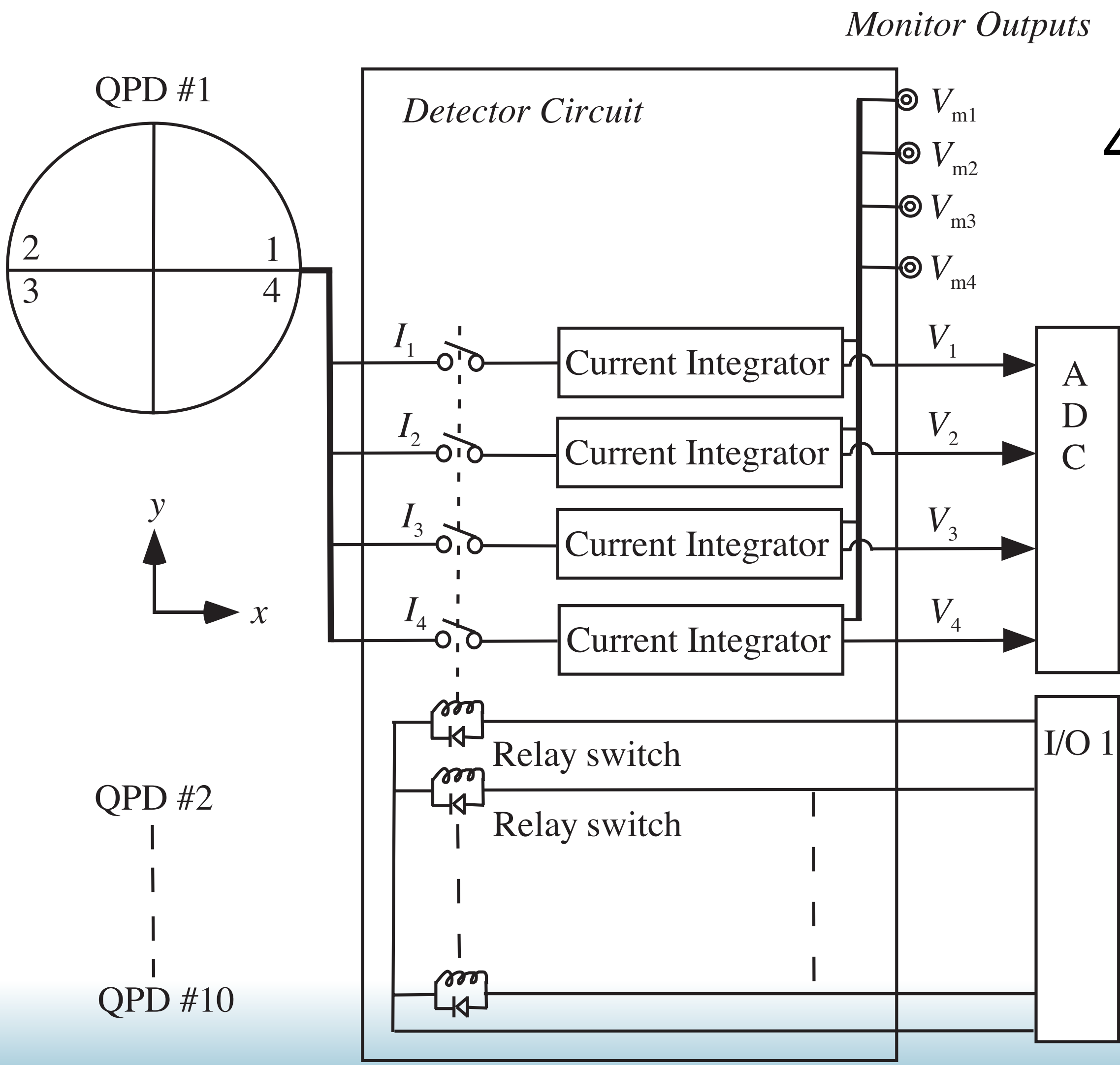

4ch ゲインバランス
< +/-0.02%

Block diagram of a local control system

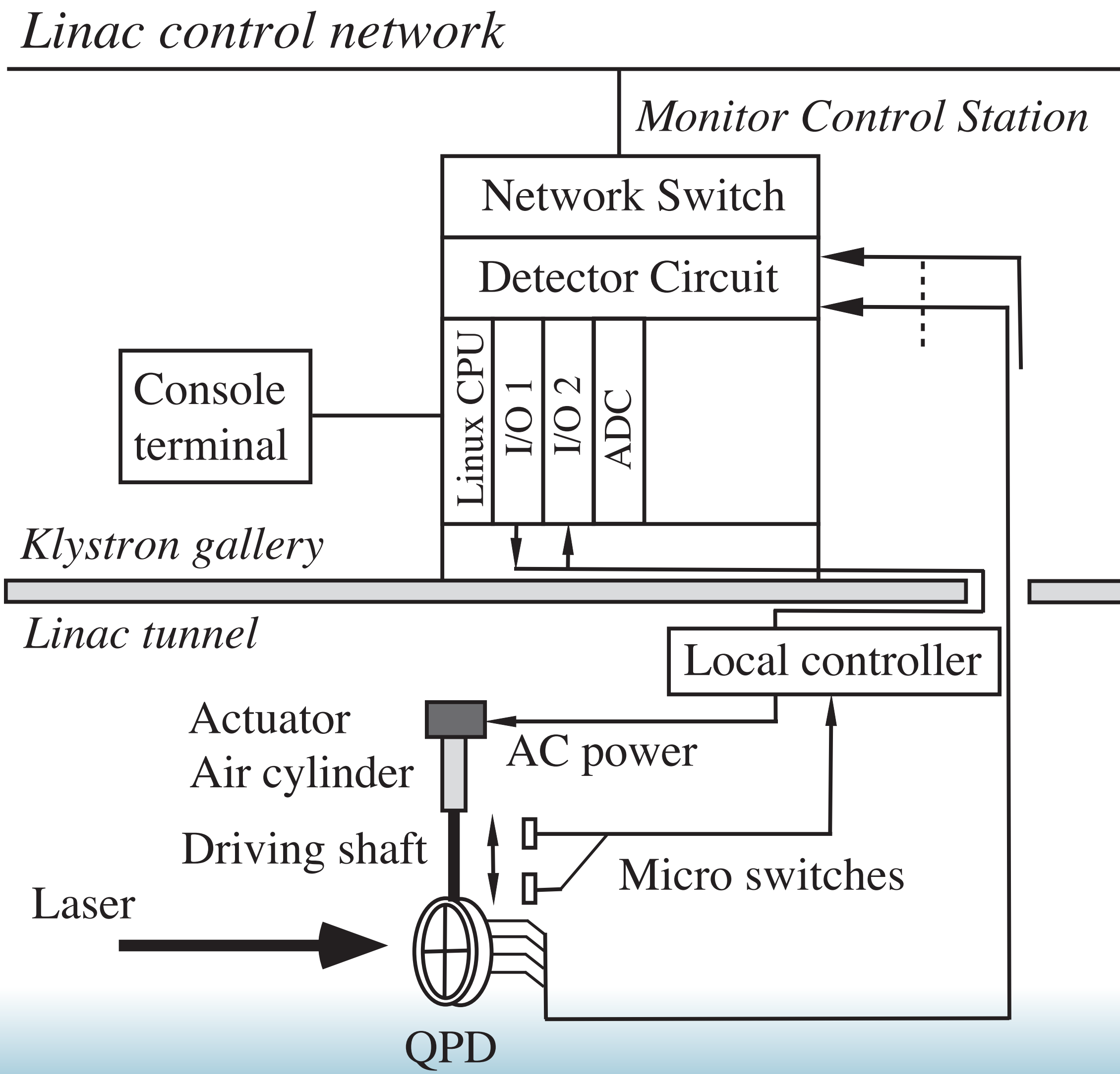

スクリーンモニターシステムと制御は共通

Expected error sources and estimations

Errors	Source of errors	rms error (μm)
Systematic error	*Mechanical*	
	• Mounting error of QPD	10
	• Mounting error of QPD holder	30
	• Reproducibility of QPD position	30
	Electrical	
	• Detection (offset) error of QPD	12
	Laser Shape	
	• Profile error	10
	Summation (rms sum)	46
Statistical error	*Laser stability*	
	• Laser axis stability	± 30

Laser window

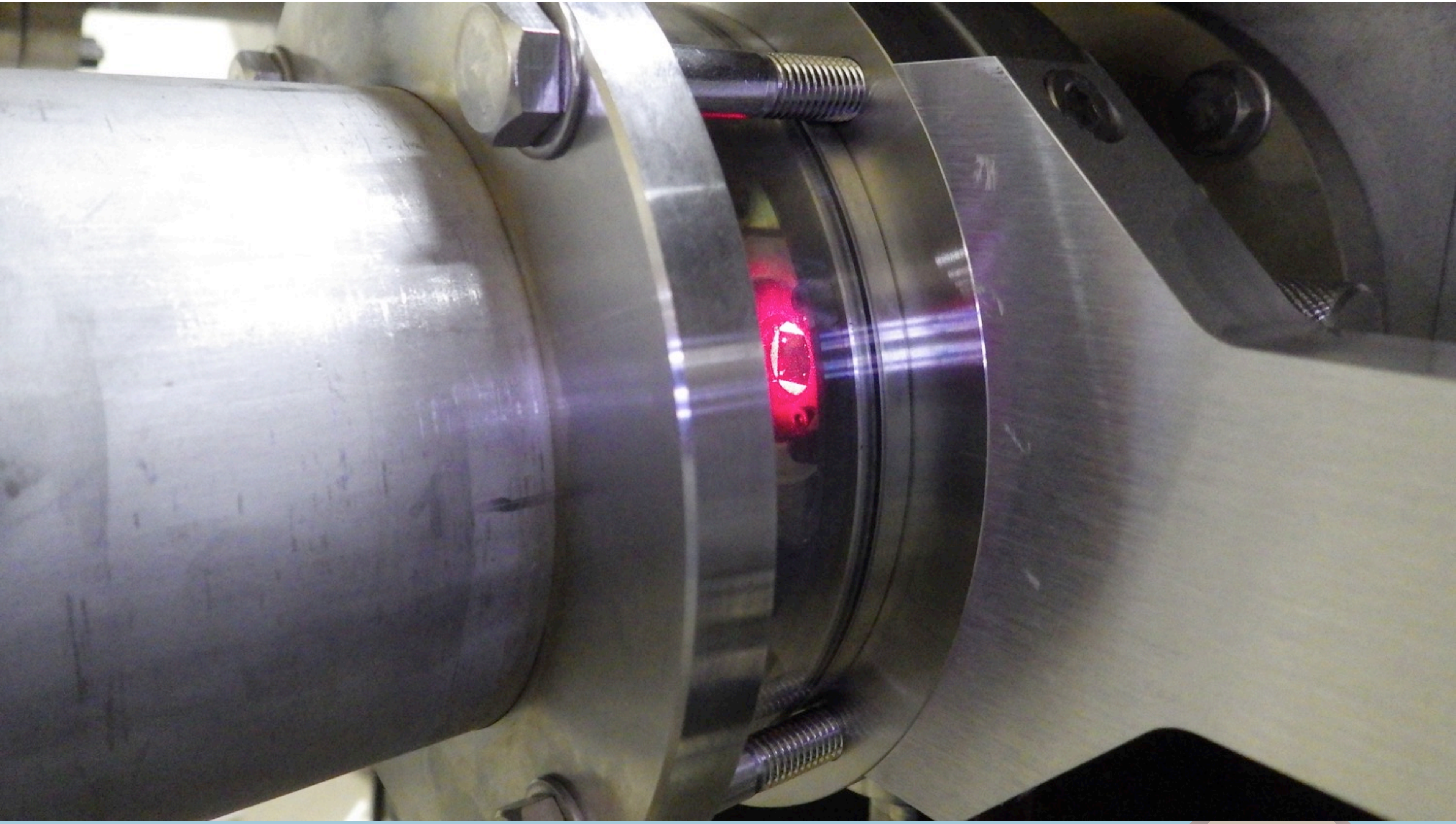

Time trace of a typical displacement vector @ QPD-38DA

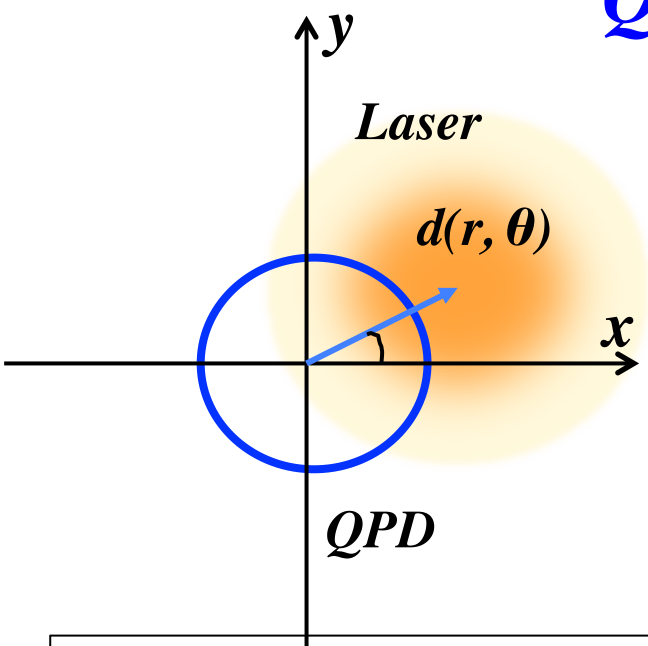

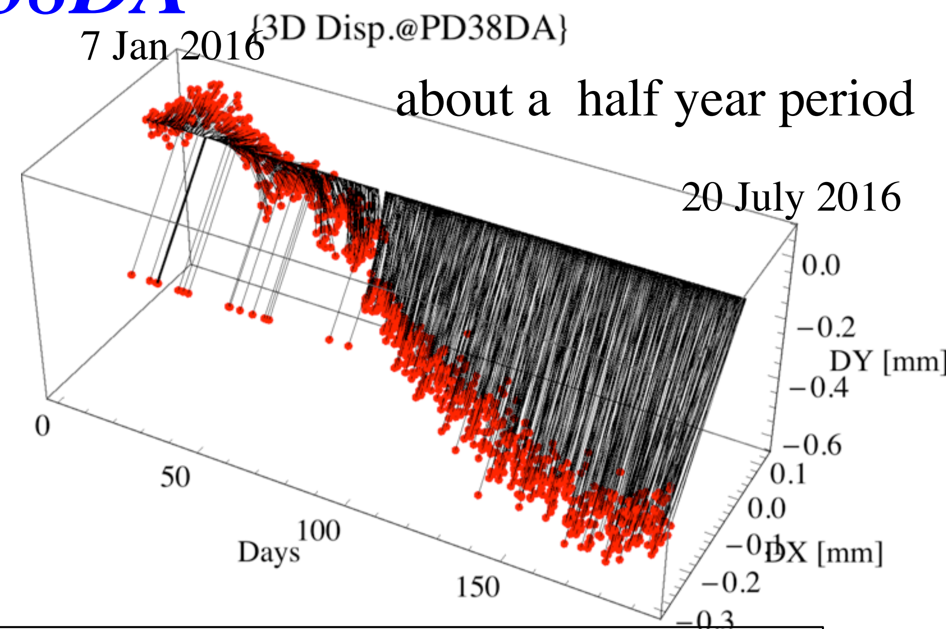

*displacement vector **d***

differential displacement vector

- Every four hours on the hour, the basic functions provided by the server start to work in order to take a series of the displacement data for all the remote QPDs.
- The results show typical variations in a time trace of the displacement vector with a feedback control on.
- It can be seen that the displacement vector has complicatedly rotated around the laser axis along with the growth of the vector norm in the time direction.

Typical displacement vectors @ QPD-38DA

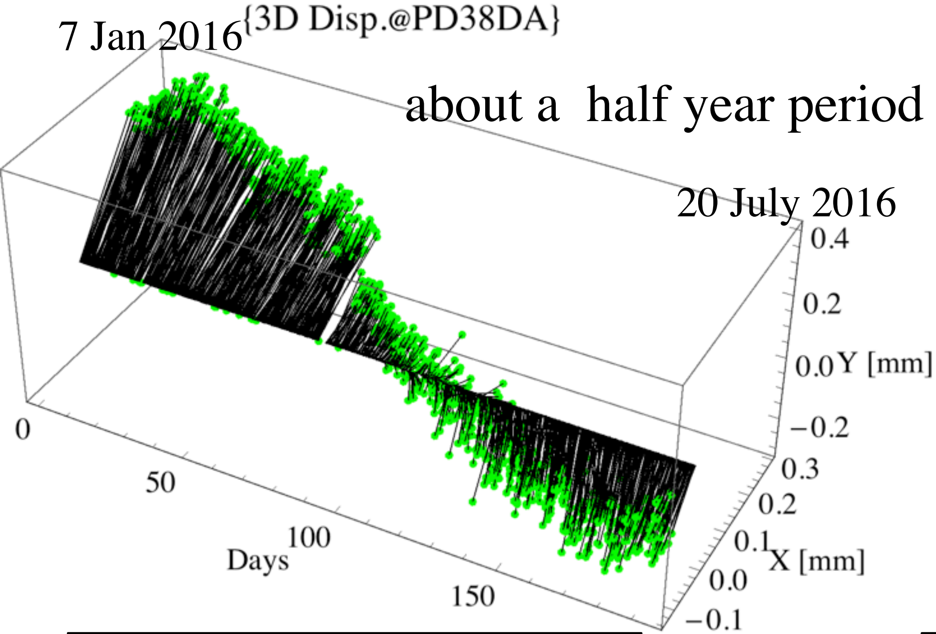

displacement vector

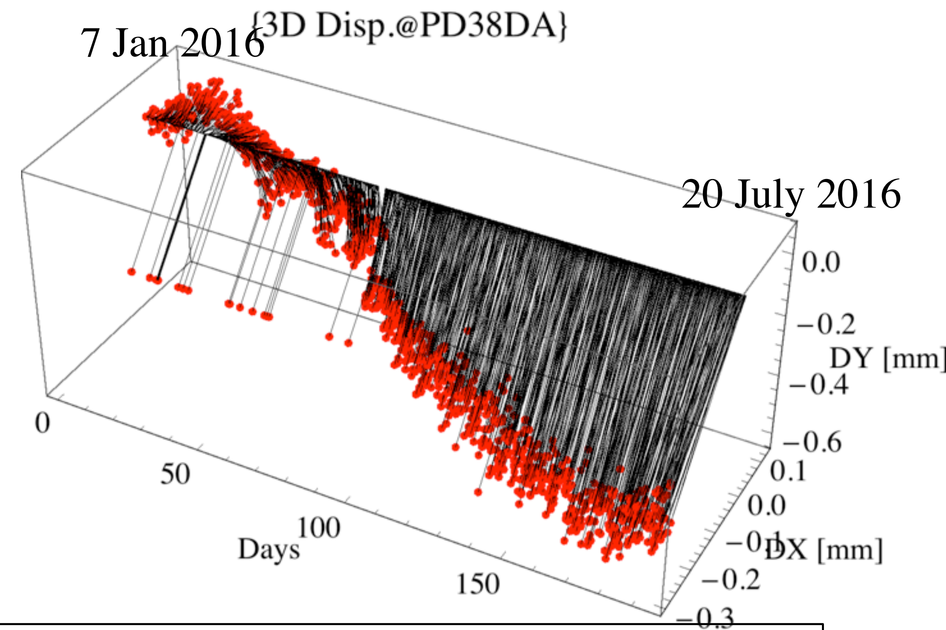

differential displacement vector

- Every four hours on the hour, the basic functions provided by the server start to work in order to take a series of the displacement data for all the QPDs.
- The results show typical variations in a time trace of the displacement vector obtained for the accelerator units with the feedback control on.
- It can be seen that the displacement vector has complicatedly rotated around the laser axis along with the growth of the vector norm in the time direction.

Introduction of the Displacement vectors

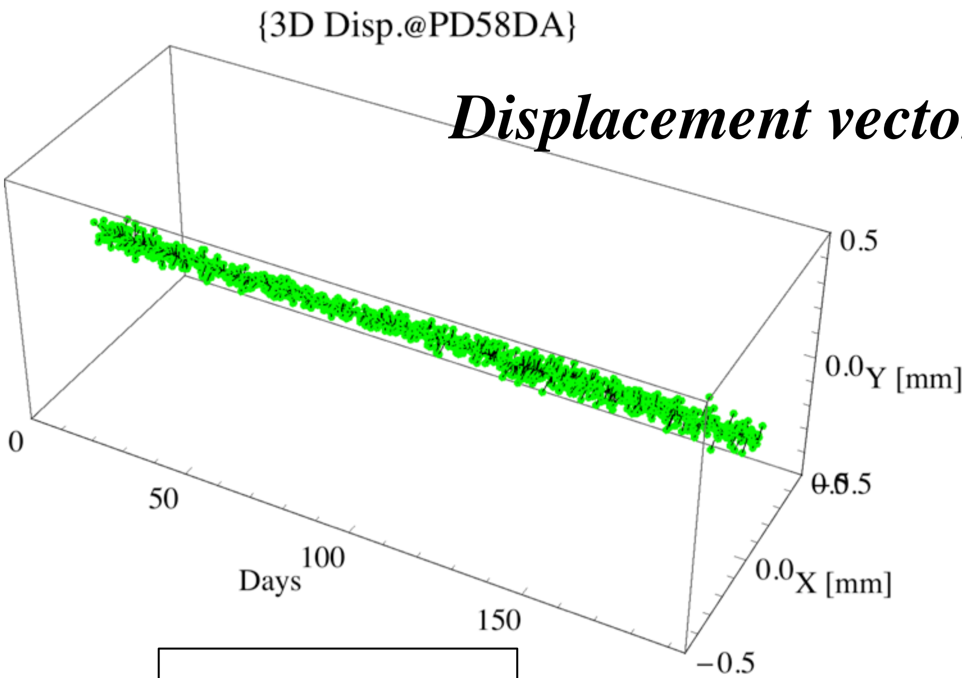

QPD_58DA

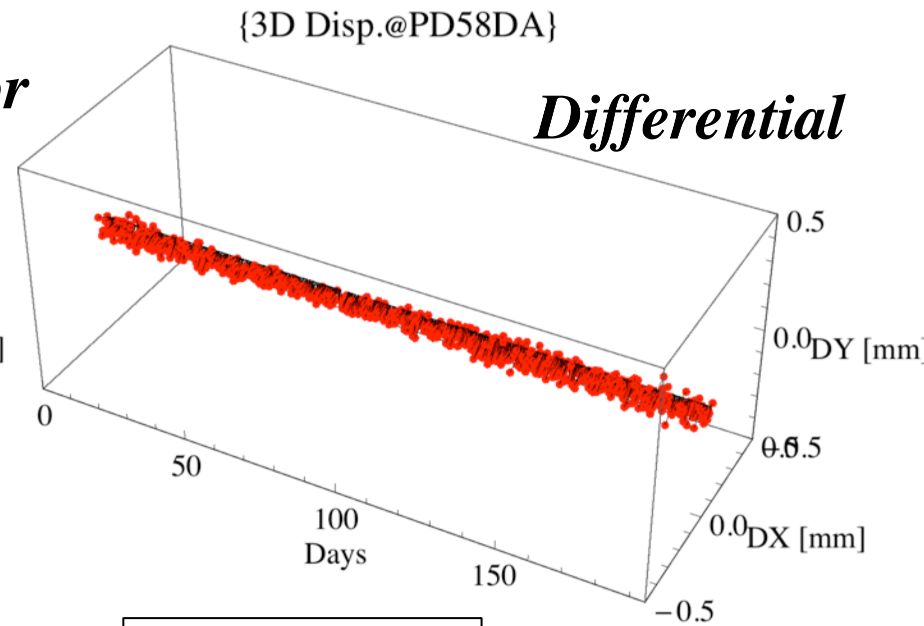

QPD_58DA

- Variations in a time trace of the displacement vector obtained for the QPD_58DA which is a feed-backed reference.

Time traces of all the displacement vectors

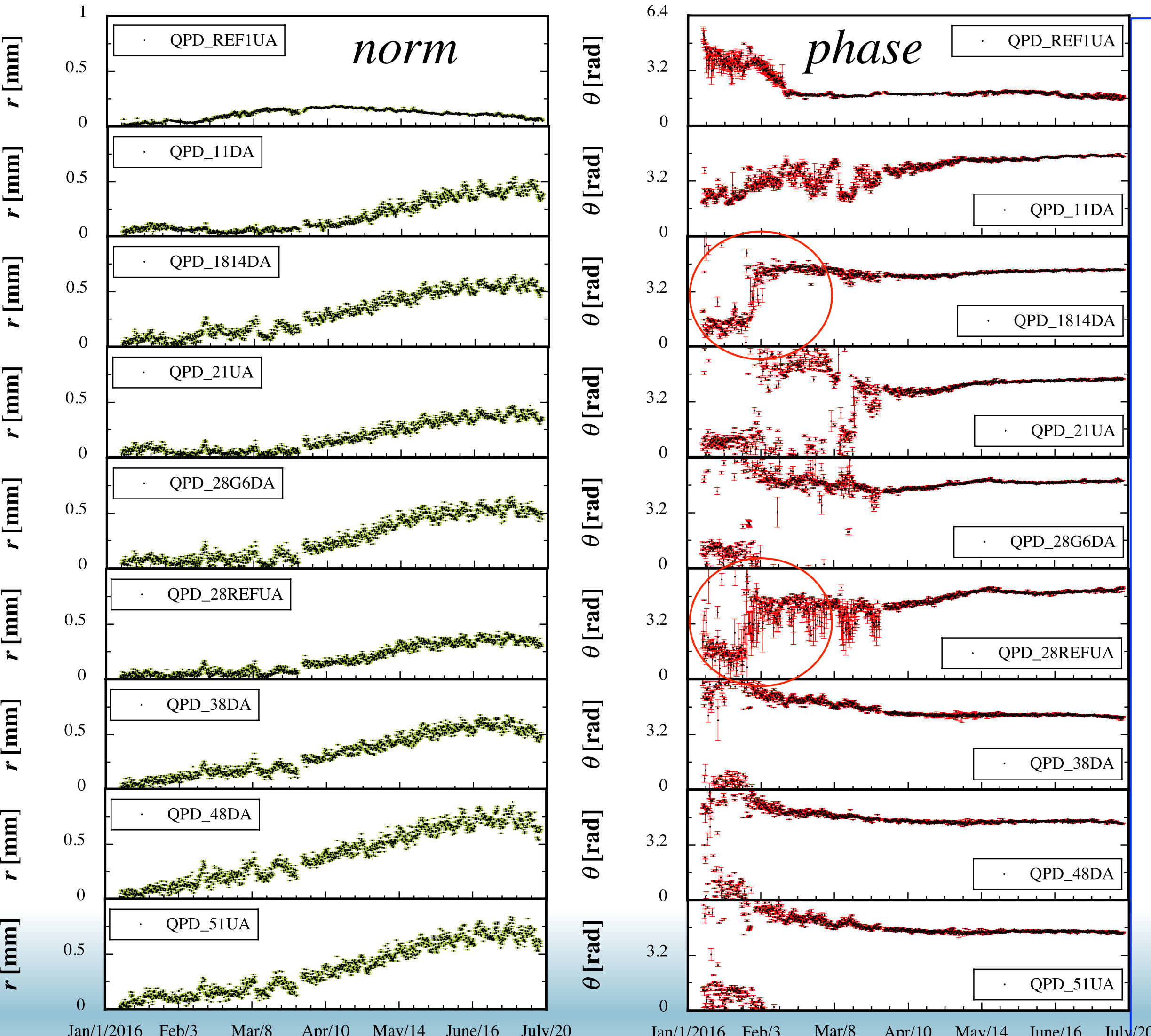

- Norm and phase of the displacement vectors for all the accelerator units with feedback control on.
- The phase is defined by an angular range of 0-2π.

- Data taking period: 7 Jan – 20 July 2016.
- *Max. norm:*
  $rmax$ = 0.19 - 0.88 mm
- *Average max. norm:*
  $<rmax>$ = 0.65 mm
- *Max. growth rate:*
  sr = 3.3 – 6.6 μm/day
- *Average max. growth rate:*
  $<sr>$ = 4.9 μm/day

Real-time measurements on dynamic floor motion

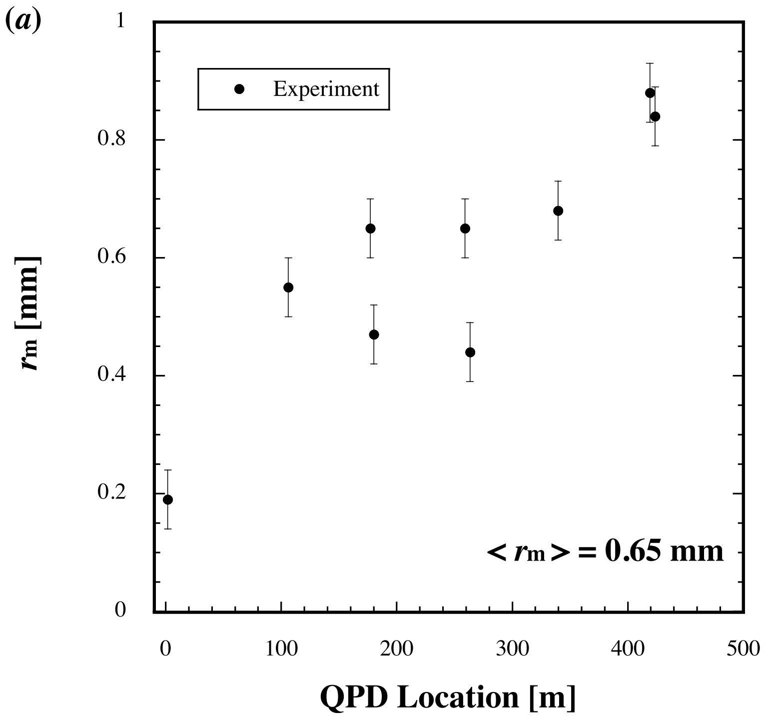

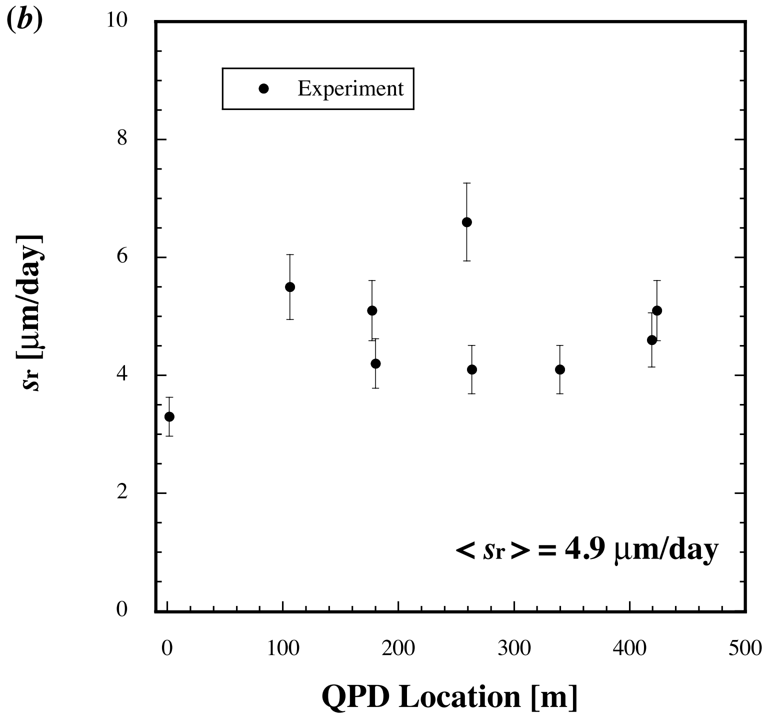

- Variations of (a) the maximum norm and (b) the maximum growth rate in the displacement vector measurements as a function of the QPD location.

Cross-correlation analysis between the displacement vectors

$$\langle \vec{\mu}(i) \rangle = \frac{1}{N} \sum_{n=1}^{N} \vec{d}_n(i), \qquad (1)$$

$$\hat{C}_k(i,j) = \frac{1}{N} \sum_{n=1}^{N} (\vec{d}_n(i) - \langle \vec{\mu}(i) \rangle) \bullet (\vec{d}_{n-k}(j) - \langle \vec{\mu}(j) \rangle), \ (2)$$

$$\hat{R}_k(i,j) = \frac{\hat{C}_k(i,j)}{\sqrt{\hat{C}_0(i,i)\hat{C}_0(j,j)}}. \qquad (3)$$

(1) $<\mu(i)>$: average of the n-th displacement vectors $d_n(i)$ of the i-th QPD in time series with a maximum data length of N.
(2) $C_k(i,j)$: cross-covariance function between the n-th displacement vectors ($d_n(i)$ and $d_n(j)$) obtained for the i-th and j-th QPDs, respectively, in time series with time lag of k.
(3) $R_k(i,j)$: cross-correlation function. $R_k(i,j)=1$ (-1) : strong positive (negative) correlation, $R_k(i,j)=0$: no correlation, $k = 0$ ($k \neq 0$) stands for the cross-correlation function at present (past) time.

Spatial cross-correlation analysis between the displacement vectors

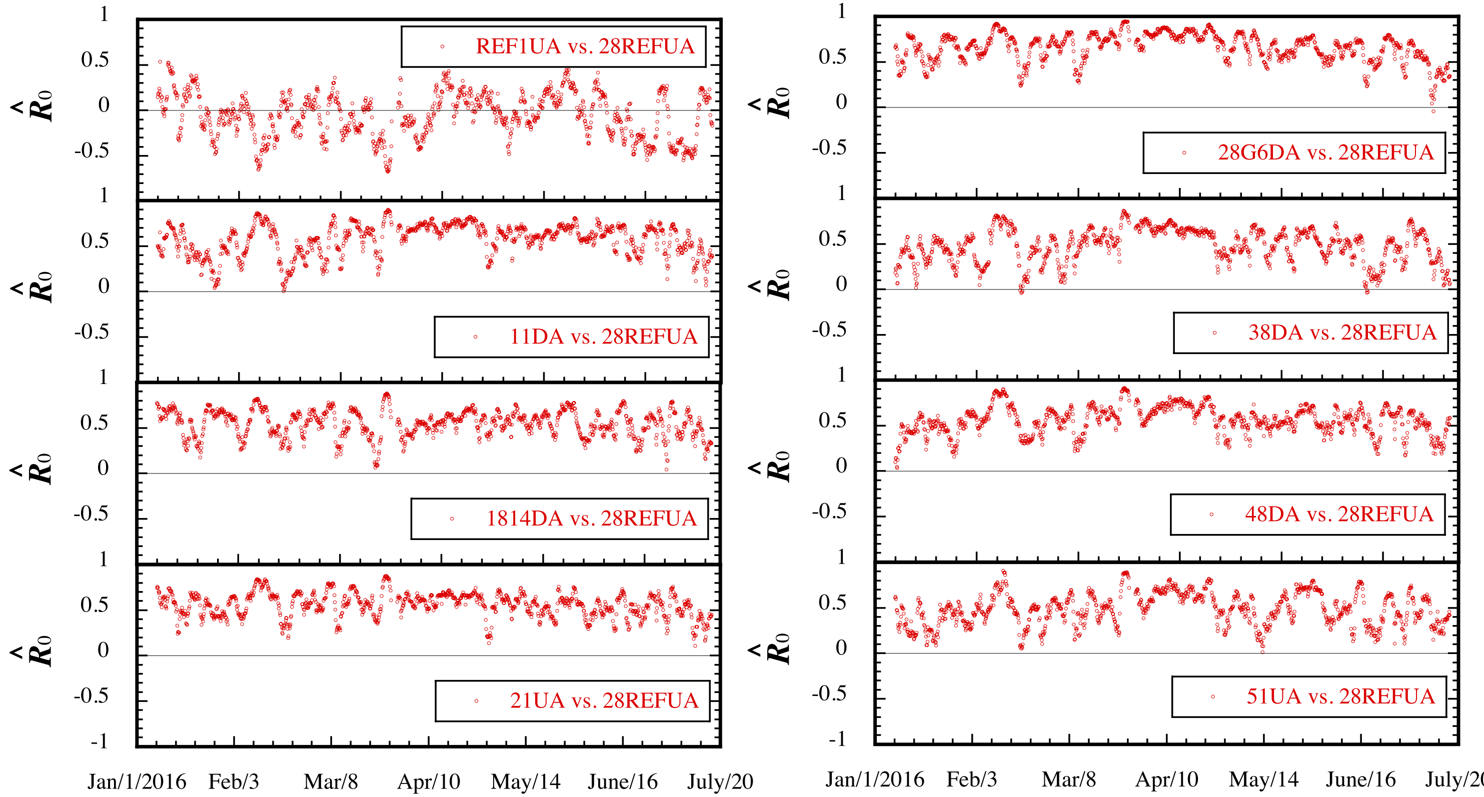

- Time traces in the spatial cross-correlation function of the displacement vectors between the reference QPD (QPD_REF28DA) and other QPDs for the accelerator units with the feedback control on during the same term.

Temporal cross-correlation analysis between the displacement vectors

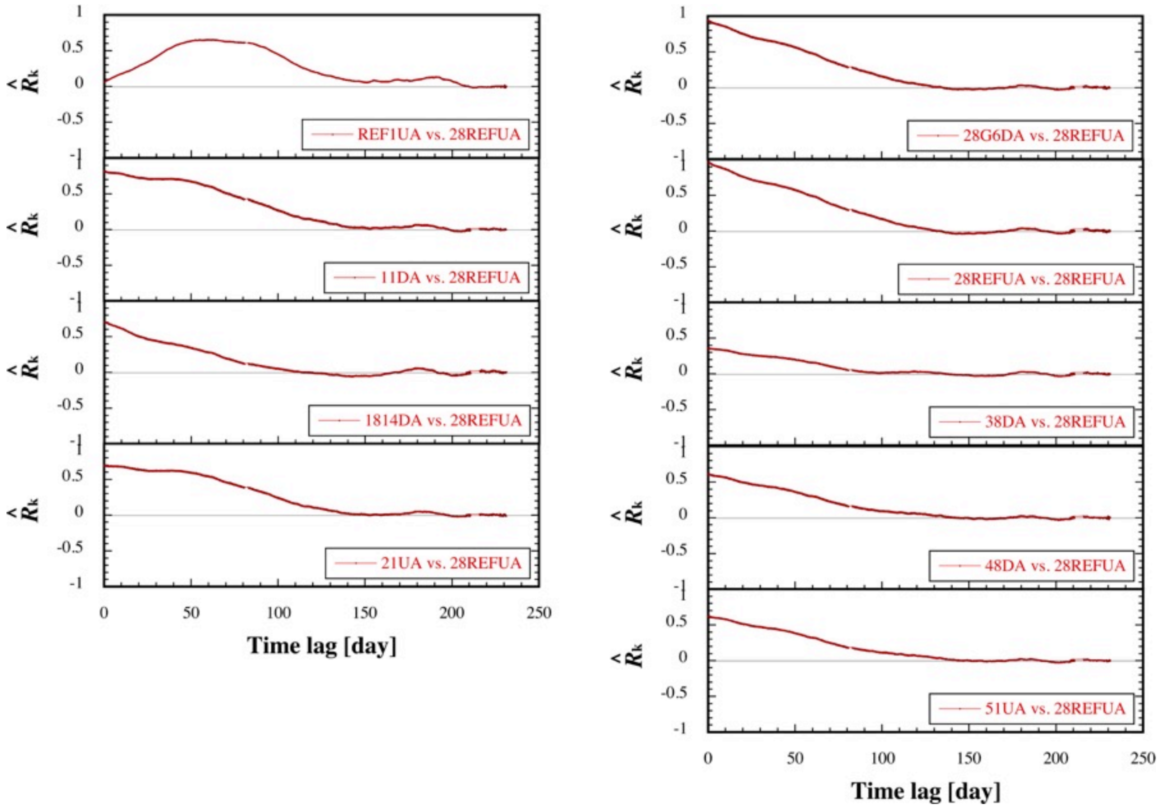

QPD_REF28DA

- Time traces in the temporal cross-correlation function of the displacement vectors between the reference QPD (QPD_REF28DA) and other QPDs for the accelerator units with the feedback control on during the same term.

Cross-correlation analysis between the displacement vectors

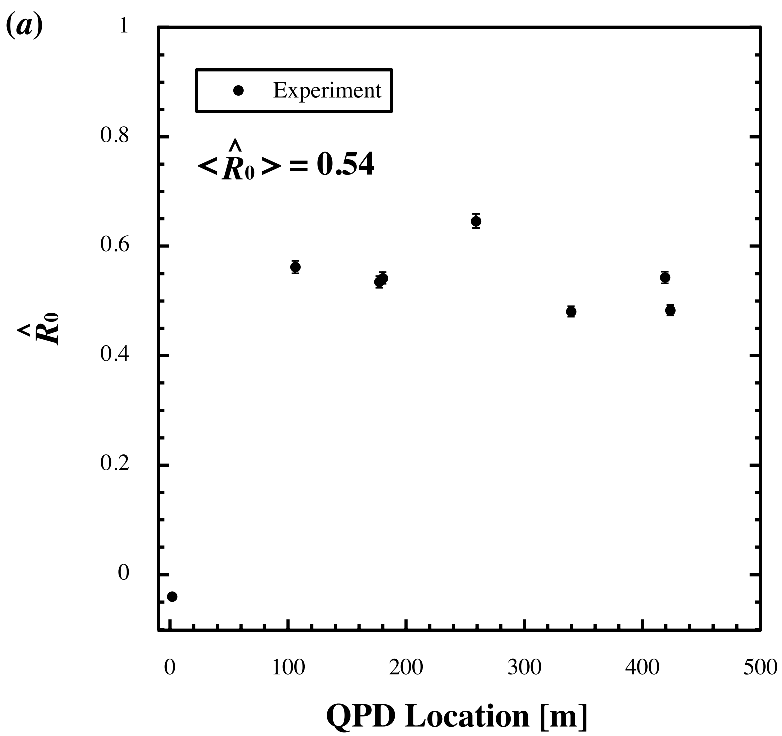

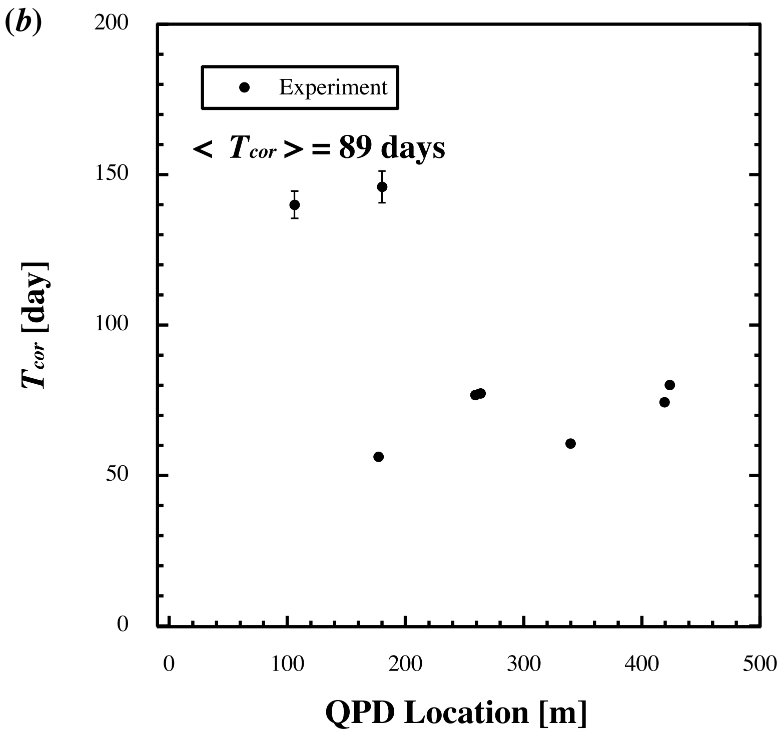

- Time traces in the spatial cross-correlation function of the displacement vectors between the reference QPD (QPD_REF28DA) and other QPDs for the accelerator units with the feedback control on during the same term.

Animations in time series for the cross-correlation analysis between the displacement vectors

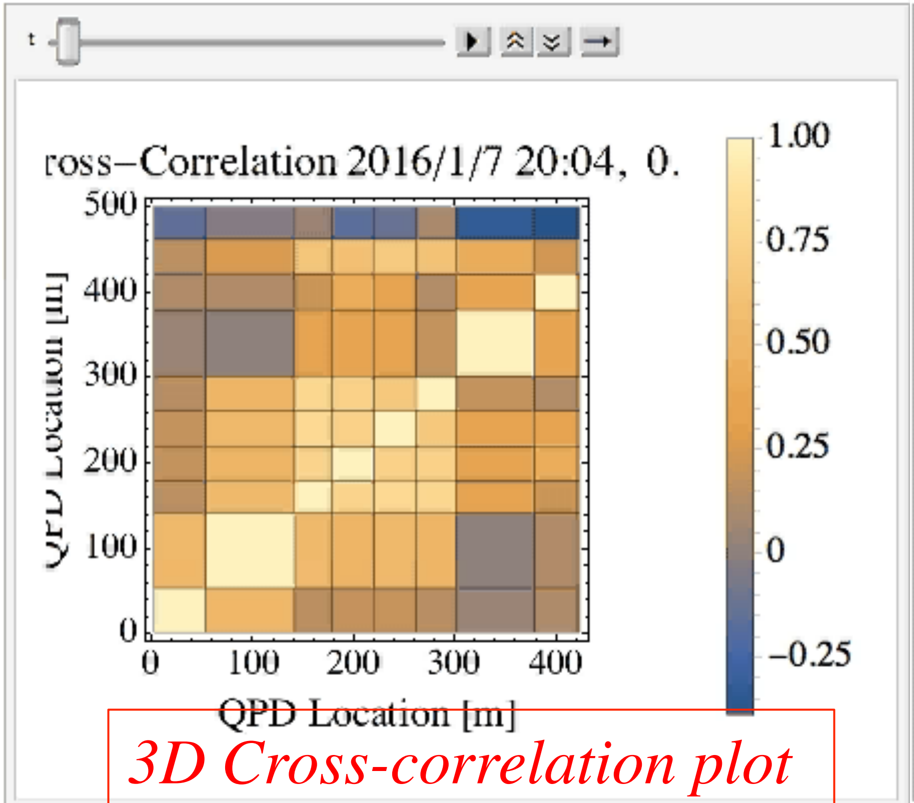

3D Cross-correlation plot

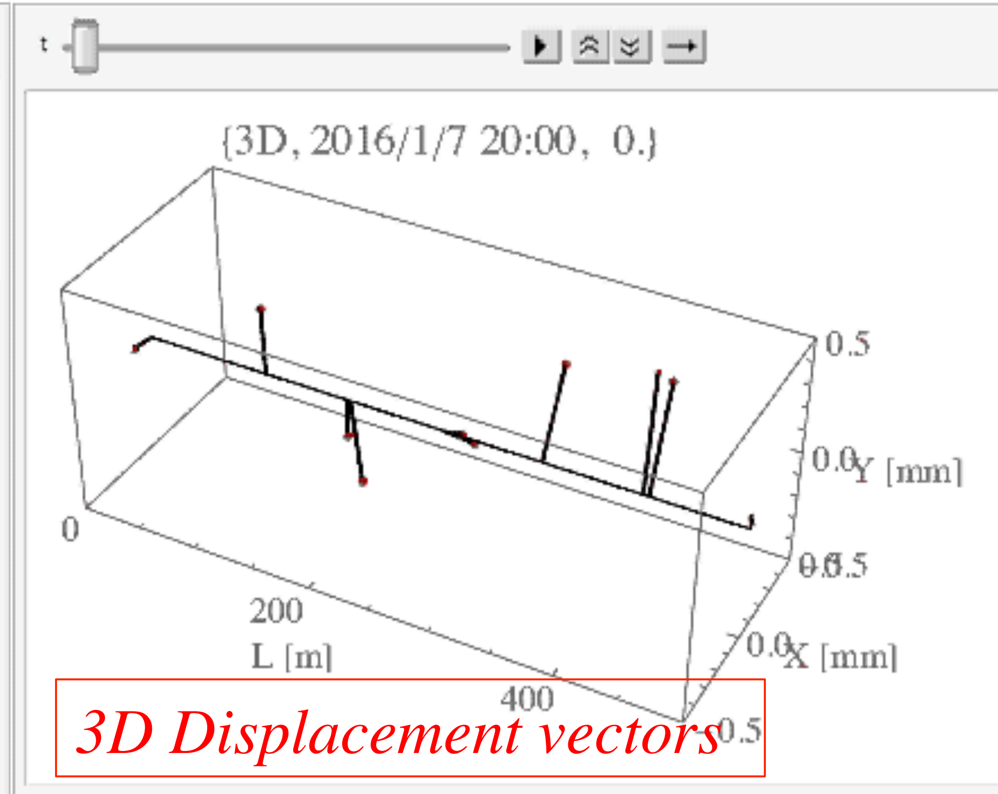

3D Displacement vectors

Real-time measurement in time series of the cross-correlation function

Real-time measurement in time series of the displacement vector

Summary

- 今後は、さらにデータを蓄積し入射器トンネルの長期変動傾向を捉えたい.
- 地面変動のブラウン運動成分（拡散成分）の定量化を行う.
- 産業応用：ダム事業、トンネル構築、堤防建設など高精度な長直尺を必要とする大規模土木事業など産業応用のみならず、地震や地殻変動を監視するための大規模観測網にも応用可能.

Back-up files

Results of the laser size measurements along the linac

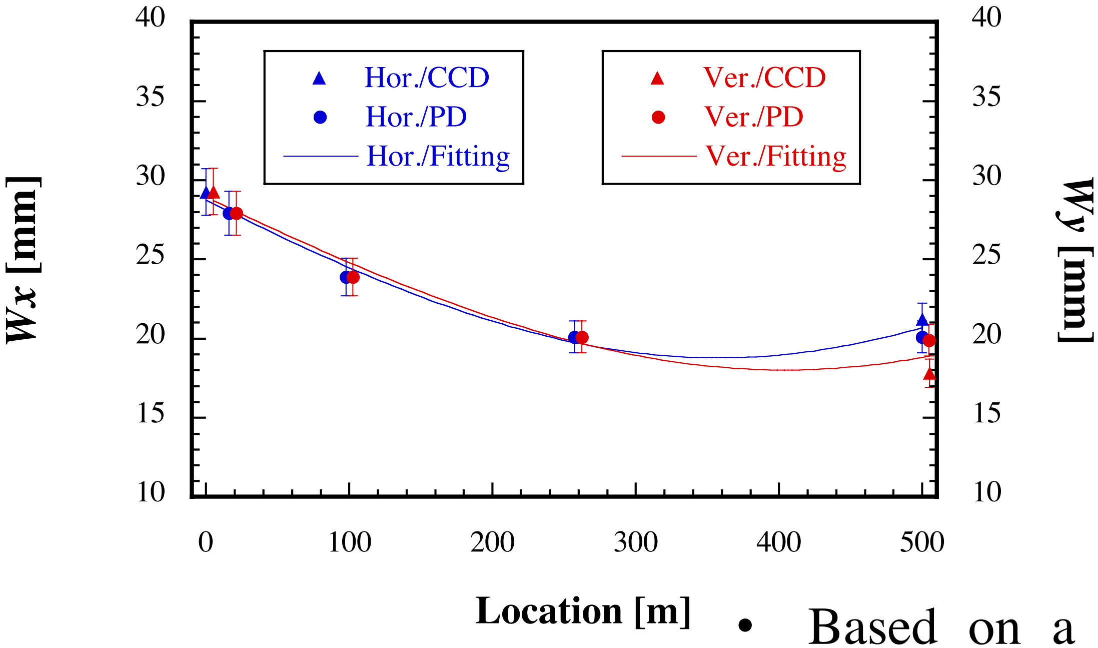

- *Direct beam size meas.*

  Δ: with CCDs at two end points
- *Indirect beam size meas.*

  •: by a mapping with a movable QPD in the x and y directions at the middle locations, while the laser axis is fixed

Fitting function

$$W_x(z) = W_{x0}\sqrt{1+\left(\frac{z-z_{x0}}{z_{Rx}}\right)^2},$$

- Based on a least-square fitting procedure with standard Gaussian laser optics, the widths propagating along the z-axis were obtained as follow:

  Rayleigh lengths z_{Rx} ~ 308 m, z_{Ry} ~ 321 m,

  Waist locations z_{x0} ~ 358 m, z_{y0} ~ 399 m,

  Beam sizes at waist locations W_{x0} ~ 18.8 mm, W_{y0} ~ 18.0 m,

Short range component alignment on the girder

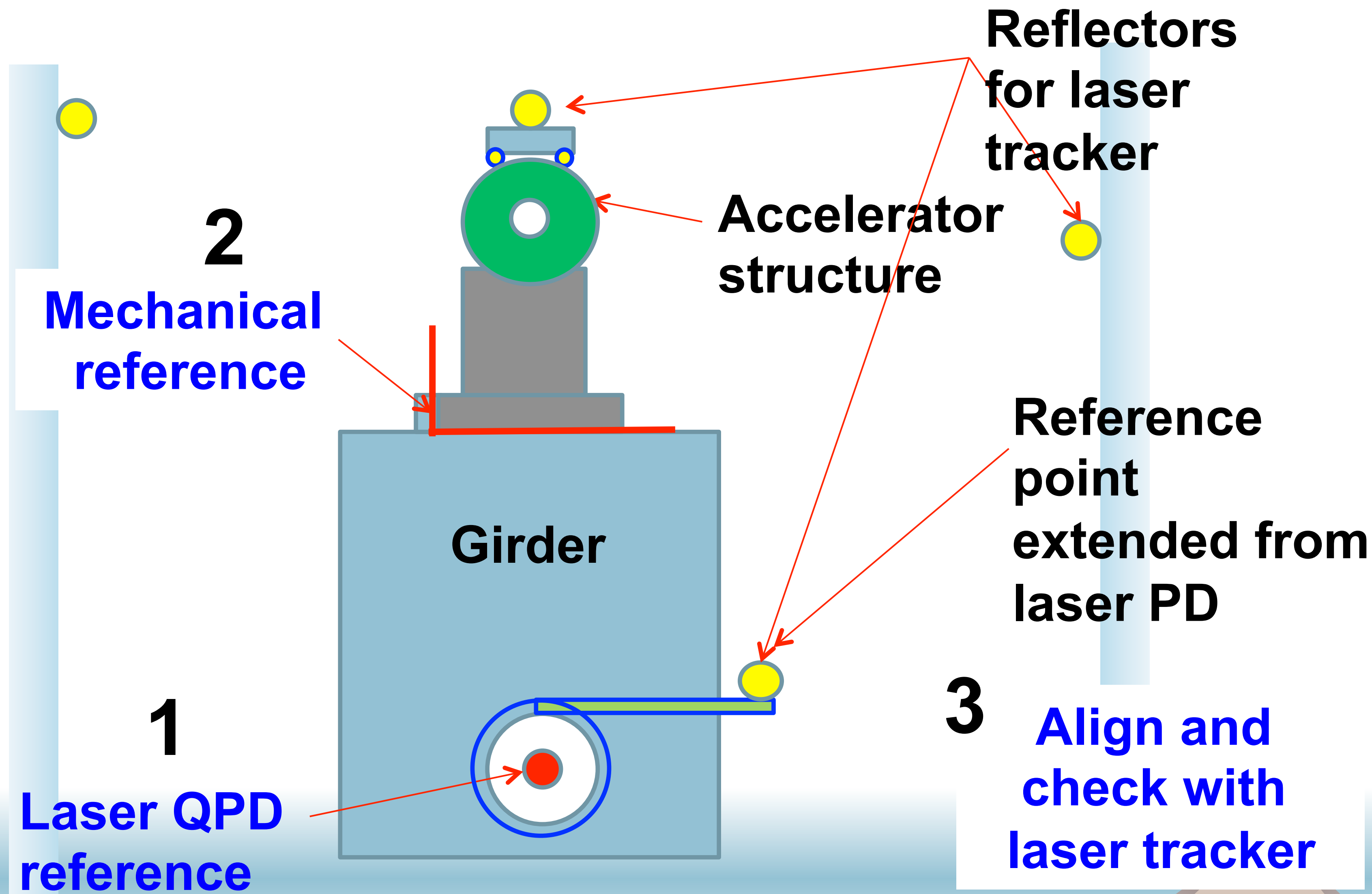

Laser system under operation

Remote-controllable QPDs installed at SY2

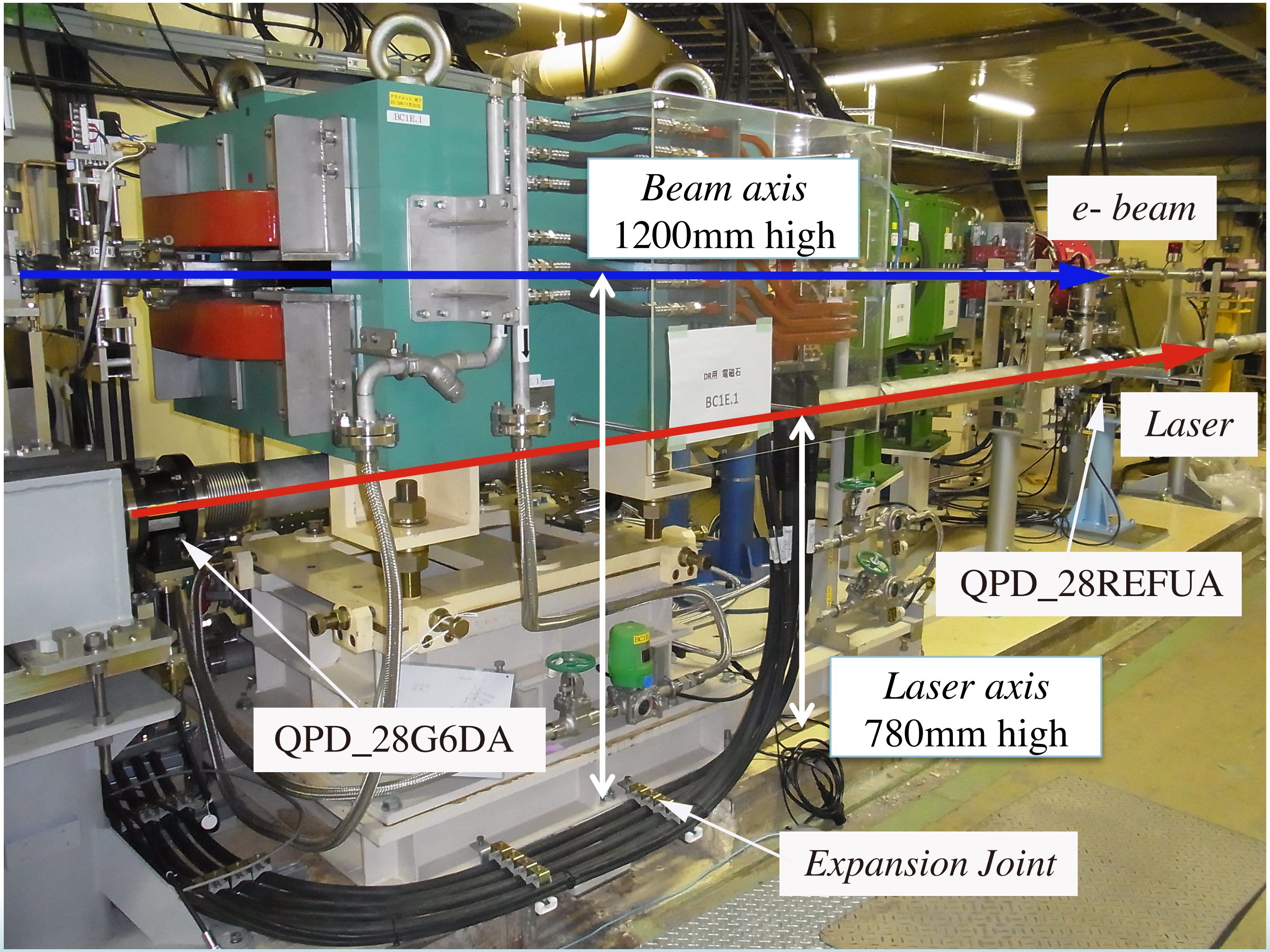

10-mW He-Ne Laser delivering

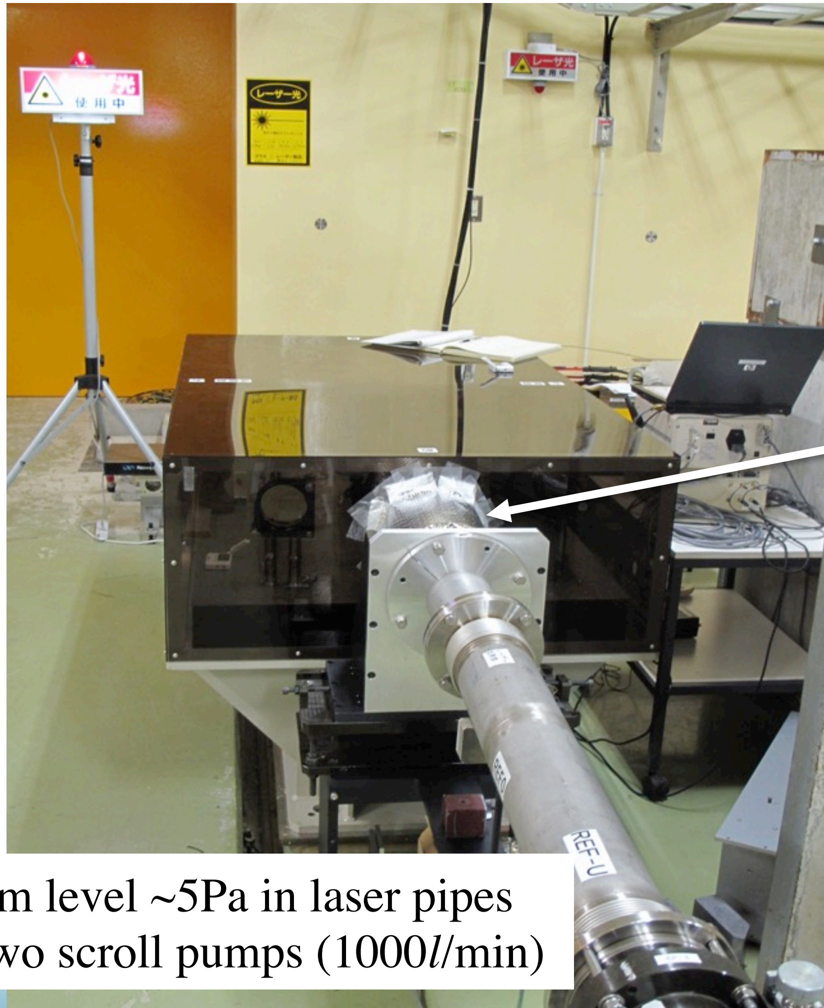

Vacuum level ~5Pa in laser pipes
with two scroll pumps (1000*l*/min)

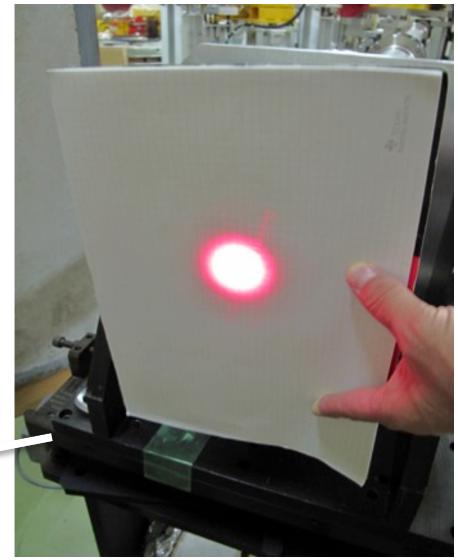

W~30mm (FW)
at the injection point

W~30mm (FW)
at the 500m-long linac
end point

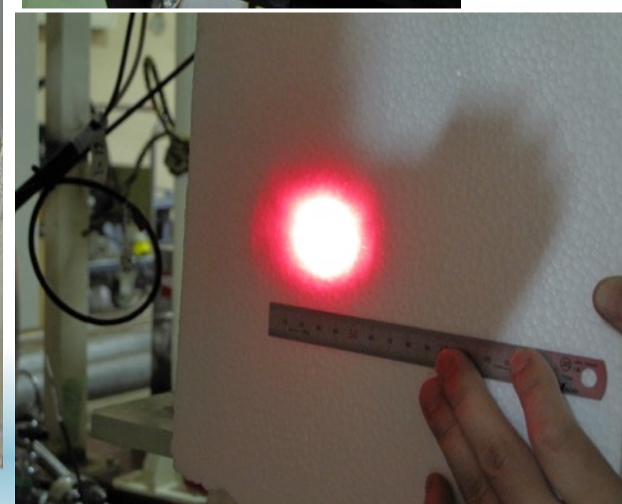

Quadrant Silicon Photo-Diode (QPD)

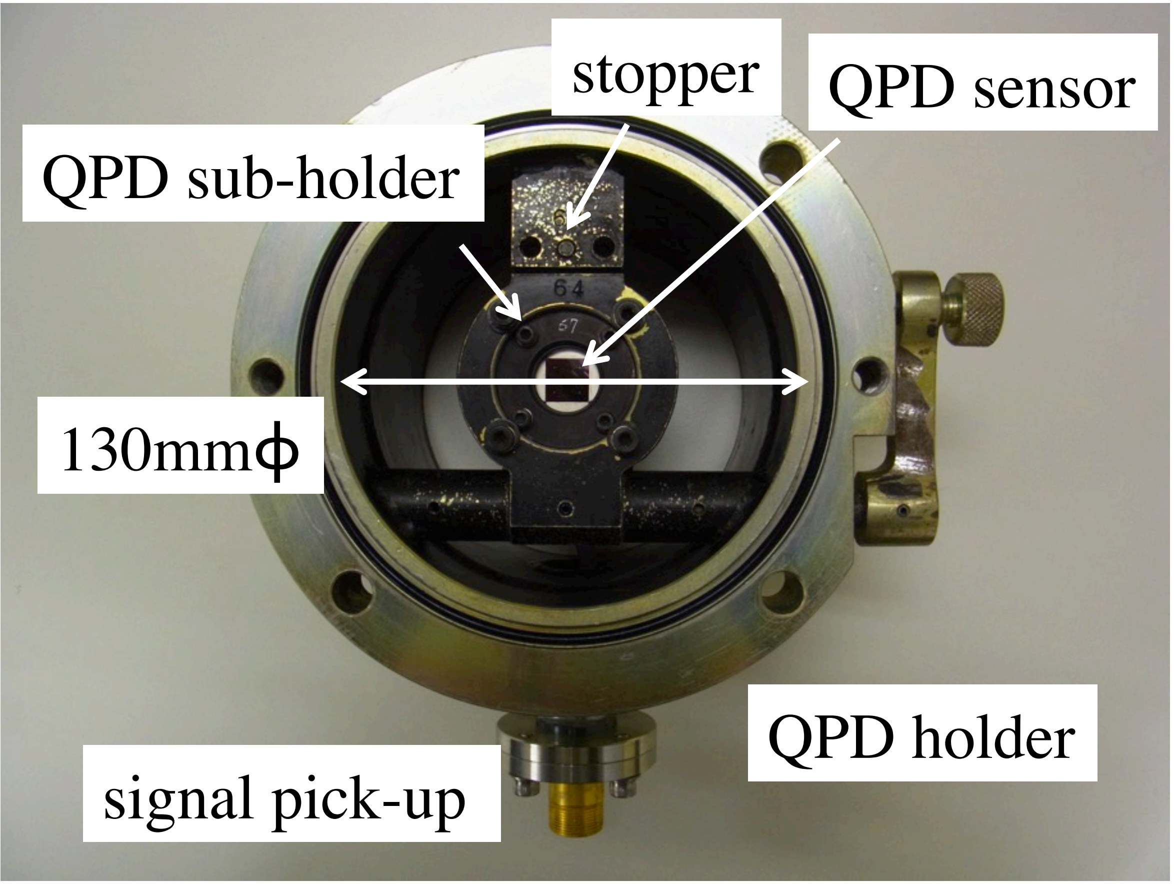

QPD target

QPD: <u>OSI Optoelectronics</u>
SPOT-9D (D=10mmϕ)

- QPD is mounted in the center of a sub-holder.
- The sub-holder can stand upright by rotation of a lever through hinge structure. The inner diameter of the holder is 130mmΦ.
- The QPD holder is connected to a laser pipe (SUS) by flange-flange joining.

Time traces of the displacement vectors (cont'd)

- It can be understood that the norms of the displacement vectors monotonically increase (except for that of QPD REF1UA), while it can be seen that there are some incomprehensible fine structures in each time trace.
- The variations in the maximum norm (*rm*) of the displacement vector in each time trace as a function of the QPD location are spread over a range of 0.19-0.88 mm during a half year period, and the average maximum norm ($\langle rm \rangle$) is 0.65 mm.
- The variations in the maximum growth rates (*sr*) in the time traces as a function of the QPD location are spread over a range of 3.3-6.6 μm/day depending on the QPD location, and the average maximum growth rate ($\langle sr \rangle$) is 4.9 μm/day.
- It can be clearly seen that relatively large stepwise jump arises on 28 January 2016 in the time traces of the phase for QPD_1814DA and QPD_28REFUA. It takes about four days in the rise time of the jump, and on the other hand, in the variations in the norms of the displacement vector during the corresponding term are less than 0.2 mm. It could be understood that during the corresponding term the displacement vector of the accelerator unit has rotated rather than increased in the transverse plane.

Cross-correlation analysis between the displacement vectors (cont'd)

- Each cross-correlation function varies *irregularly* in the corresponding time trace, and however, the averages in the time traces decrease in the range of $R_0 = 0.67$ to 0.48 in accordance with the distance from the reference QPD (except for QPD REF1UA where $R_0 = 0.06$).

- Relatively strong positive cross-correlations show high coherency on average in dynamic displacements of the tunnel floor in the time series along the entire length of the linac tunnel (except for QPD REF1UA).

- It should be noted that the time trace in the cross-correlation function for QPD_REF1UA is markedly different from those in the other cross-correlation functions. It seems for QPD_REF1UA to stand alone from the other building blocks.

Cross-correlation analysis between the displacement vectors (cont'd)

- The 500-m-long linac building has two floors, which together constitute the klystron gallery and the in-ground tunnel.
- The linac building comprises eight building blocks that are joined to be linearly aligned with seven expansion joints, which can absorb a certain amount of elastic deformation caused by expansion or contraction of the building blocks.
- However, residual amounts of elastic deformation may induce deformation of the building blocks themselves. This may increase the displacement of the accelerator units through displacements of the tunnel floor, triggered by the complex processes that were mentioned previously.
- In particular, it should be noted that the fiducial points created by the laser axis can move dynamically and independently in proportion to the displacement vector of the tunnel floor, even though the last fiducial point is strictly fixed at the last QPD center with the feedback control on.
- Thus, the laser axis itself cannot become an entirely fixed and stable fiducial axis as an absolute fiducial line, because it is not possible to directly stabilize dynamic ground motion.

Data-taking procedure on the real-time measurement

- Every four hours on the hour, the basic functions provided by the server start to work in order to take a series of the displacement data for all the QPDs.
- The basic functions comprise
  - a) ***feedback control for the laser axis***, the end positions of the laser axis at the last QPD are stabilized by the feedback control until the transverse positions of the laser axis are within the allowable region of ±50 μm from the center of the last QPD.
  - b) ***actuator control for the QPD***, the first upstream QPD is driven to the central position of the laser pipe.
  - c) ***data taking for the QPD***, displacement data of the QPD are repeatedly taken one thousand times, then average and standard deviation are calculated by using the four output voltages along with the x and y displacements.

The Super KEKB : an electron-positron collider with asymmetric energies

I_b =3.6A positron beam

e^+ $E = 4$ GeV

e^- $E = 7$ GeV

I_b =2.6A electron beam

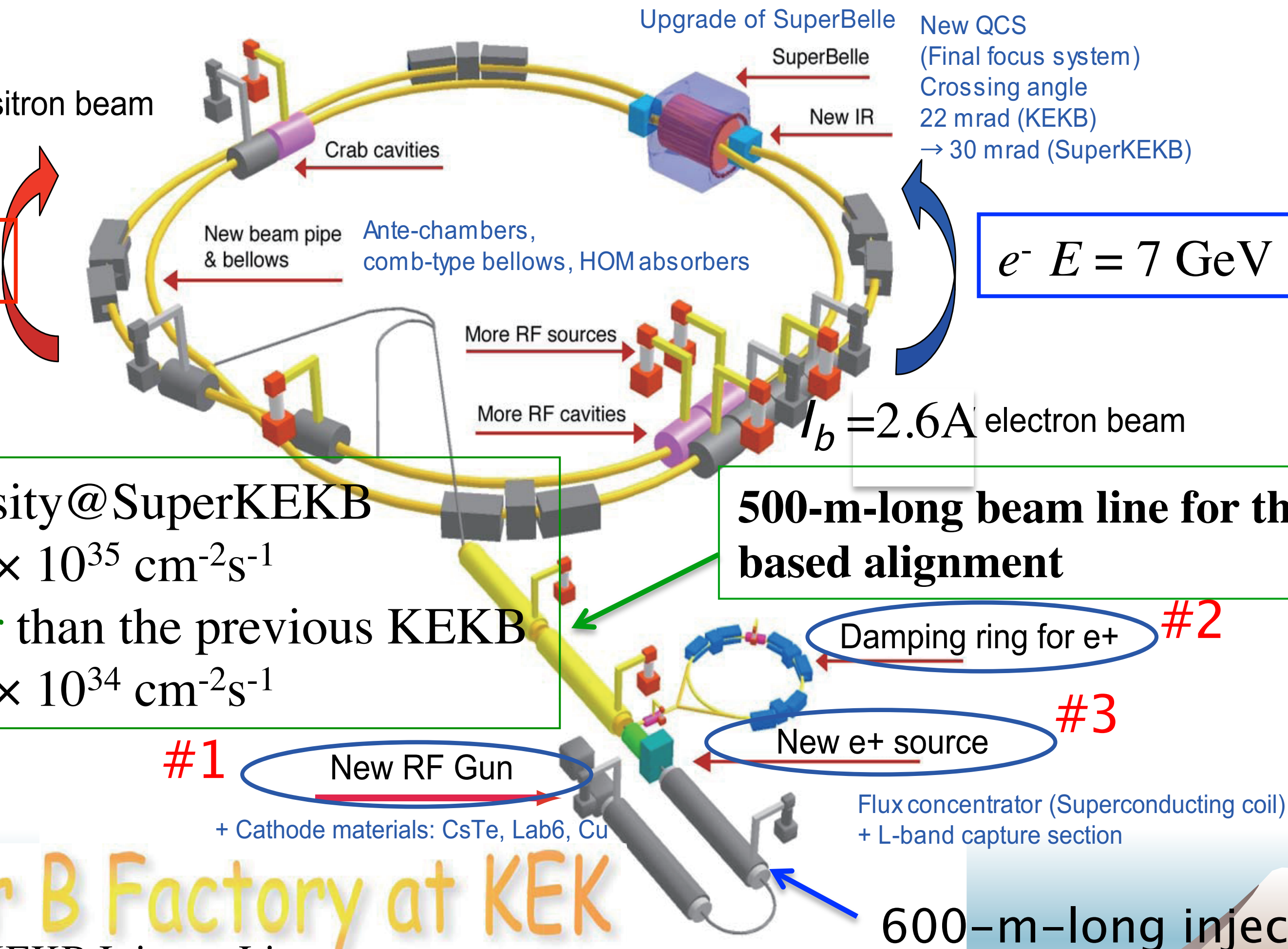

Target Luminosity@SuperKEKB

$$L = 8 \times 10^{35}\ \mathrm{cm^{-2}s^{-1}}$$

40 times higher than the previous KEKB

$$L = 2 \times 10^{34}\ \mathrm{cm^{-2}s^{-1}}$$

500-m-long beam line for the laser-based alignment

Tsuyoshi Suwada /
KEKB Injector Linac

Position displacement distributions of the laser axes for 500-m-long straight line

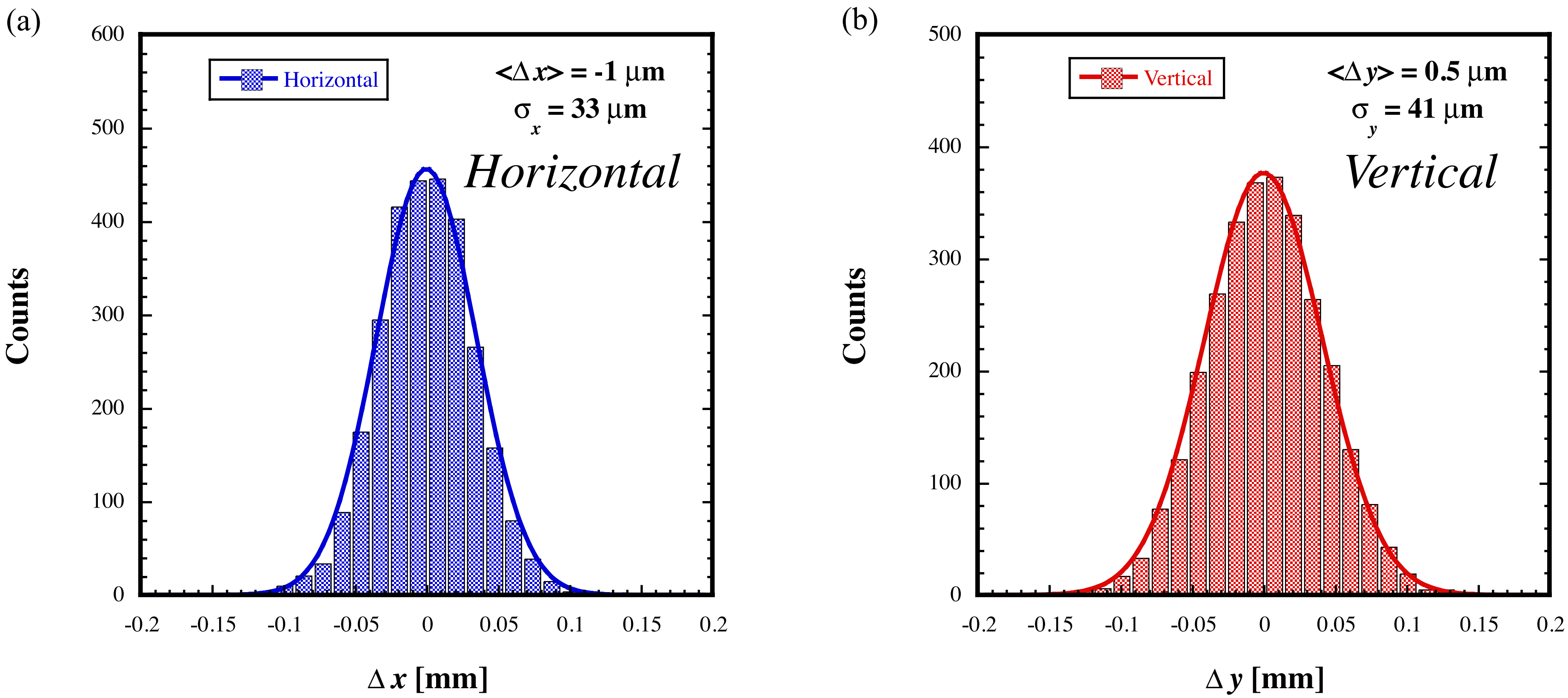

QPD Tests on radiation hardness

PD /r. r. (%)	1st. (Apr/26-May/19)	2nd. (Apr/26-June/02)	3rd. (Apr/26-June/16)	4th. (Apr/26-June/30)
O 社 PD Ch1	7.5	1.9	4.8	34
Ch2	8.5	1.5	0.67	28
Ch3	3.7	-5.1	12	28
Ch4	5.7	4.9	8.6	35
S1227-66BR	0.28	0.84	0.14	5.6
S5106	8.0	12.	18	95

Table.1 Test results of radiation hardness for several QPD samples at the KEKB injector linac. The value is indicated by the reduction rate (r. r.%) of the output voltage before radiation exposure to that after radiation exposure.

Present QPD,
OSI (SPOT-9D)

Hamamatsu
~6 times rad. hard

The samples for the 1st, 2nd, and 3rd measure
positron separator, and however, the samples f
positron target. All the samples were exposed
nominal operation condition.

HAMAMATSU
PHOTON IS OUR BUSINESS

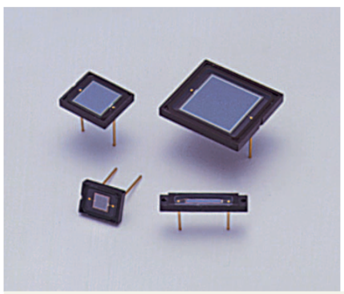

Siフォトダイオード

S1227シリーズ

紫外〜可視域精密測光用、赤外感度抑制タイプの
フォトダイオード

Cross-correlation analysis between the displacement vectors

$$\langle\vec{\mu}(i)\rangle = \frac{1}{N}\sum_{n=1}^{N}\vec{d}_n(i), \qquad (1)$$

$$\hat{C}_k(i,j) = \frac{1}{N}\sum_{n=1}^{N}(\vec{d}_n(i)-\langle\vec{\mu}(i)\rangle)\bullet(\vec{d}_{n-k}(j)-\langle\vec{\mu}(j)\rangle), \quad (2)$$

$$\hat{R}_k(i,j) = \frac{\hat{C}_k(i,j)}{\sqrt{\hat{C}_0(i,i)\hat{C}_0(j,j)}}. \qquad (3)$$

(1) $<\mu(i)>$: average of the n-th displacement vectors $d_n(i)$ of the i-th QPD in time series with a maximum data length of N.
(2) $C_k(i,j)$: cross-covariance function between the n-th displacement vectors ($d_n(i)$ and $d_n(j)$) obtained for the i-th and j-th QPDs, respectively, in time series with time lag of k.
(3) $R_k(i,j)$: cross-correlation function. $R_k(i,j)=1$ (-1) : strong positive (negative) correlation, $R_k(i,j)=0$: no correlation, $k=0$ ($k\neq 0$) stands for the cross-correlation function at present (past) time.

Cross-correlation analysis between the displacement vectors (cont'd)

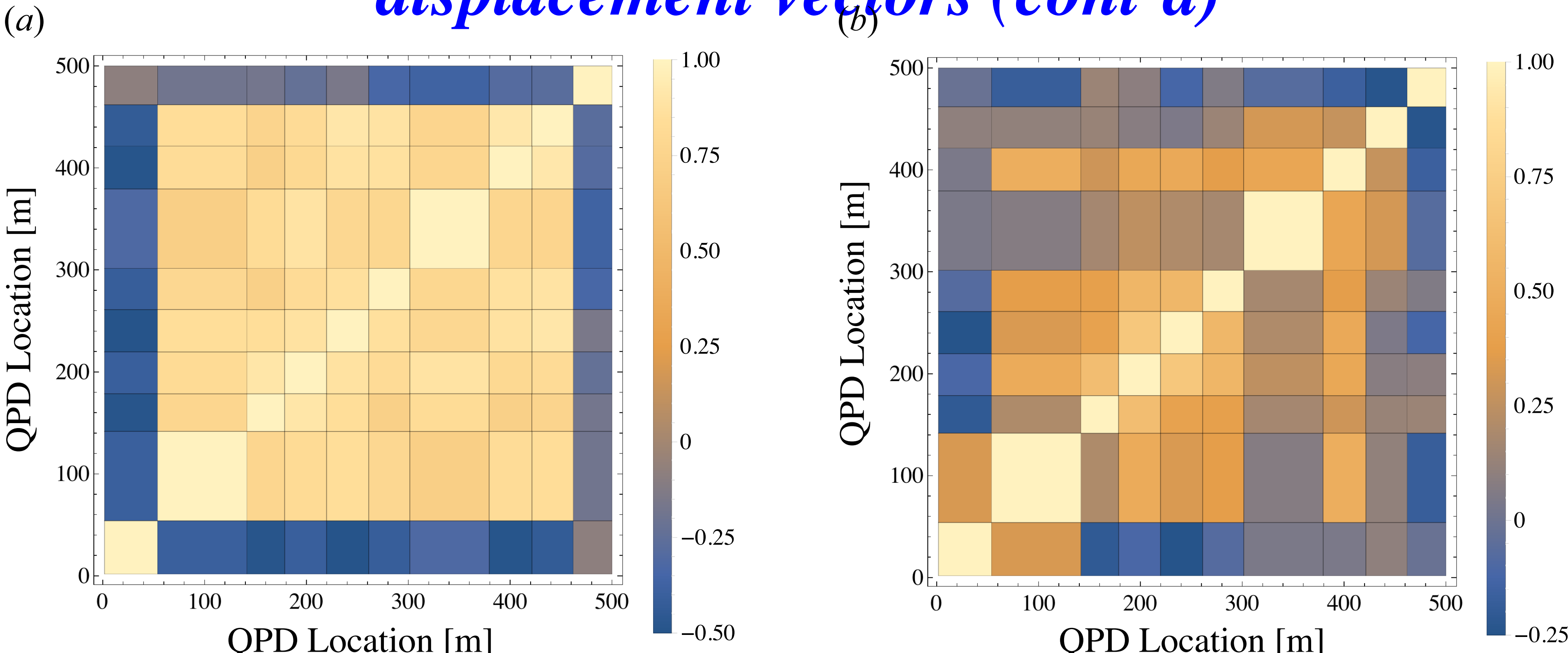

- Intensity distributions in the cross-correlation function between all the QPDs in the displacement vector measurements of the accelerator units along the C5 straight section obtained on (a) 15 February 2016 at 0:00 am and (b) 27 February 2016 at 8:00 am. The intensity distribution pattern in the cross-correlation function is linearly encoded by the color scale.

Laser size measurements along the linac

- The beam widths were directly measured at the two fiducial points (z=0 and z=500m).
- At other locations, they were analyzed by taking mapping data obtained with the help of mechanically movable QPDs while the laser beam was fixed. The mapping data were obtained by measuring the variations in the signal levels obtained from the QPD depending on the transverse displacements with respect to the fiducial line.
- The beam widths were analyzed by a least-square fitting procedure with a two-dimensional Gaussian function for the obtained mapping data.

Reference target for component alignment on the girder

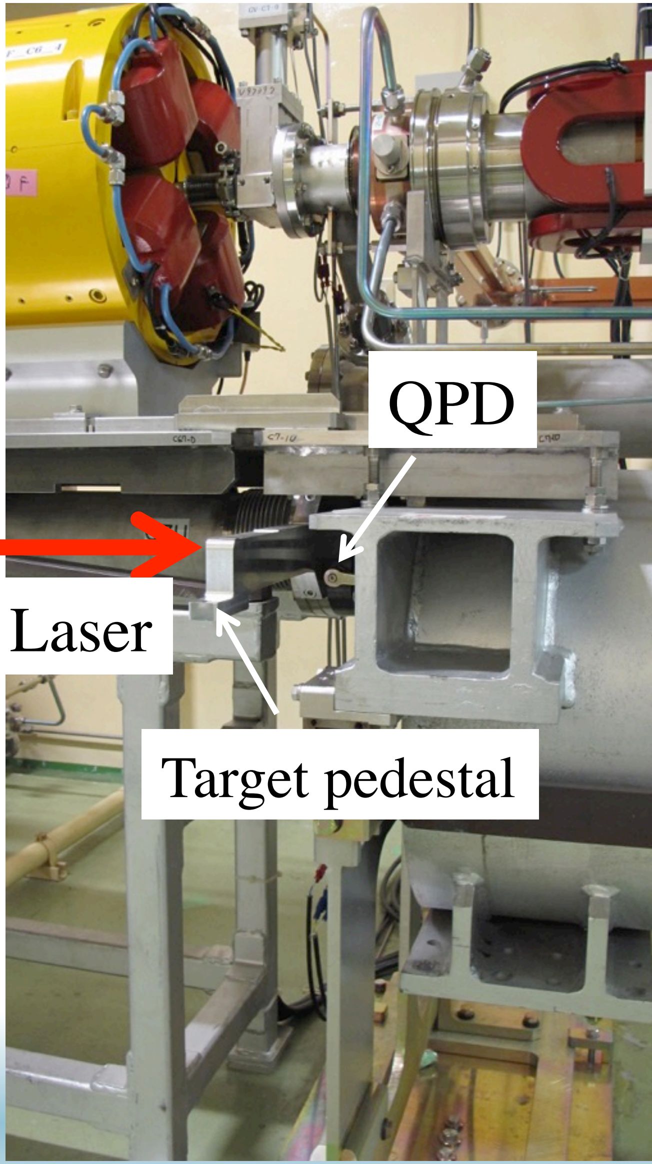

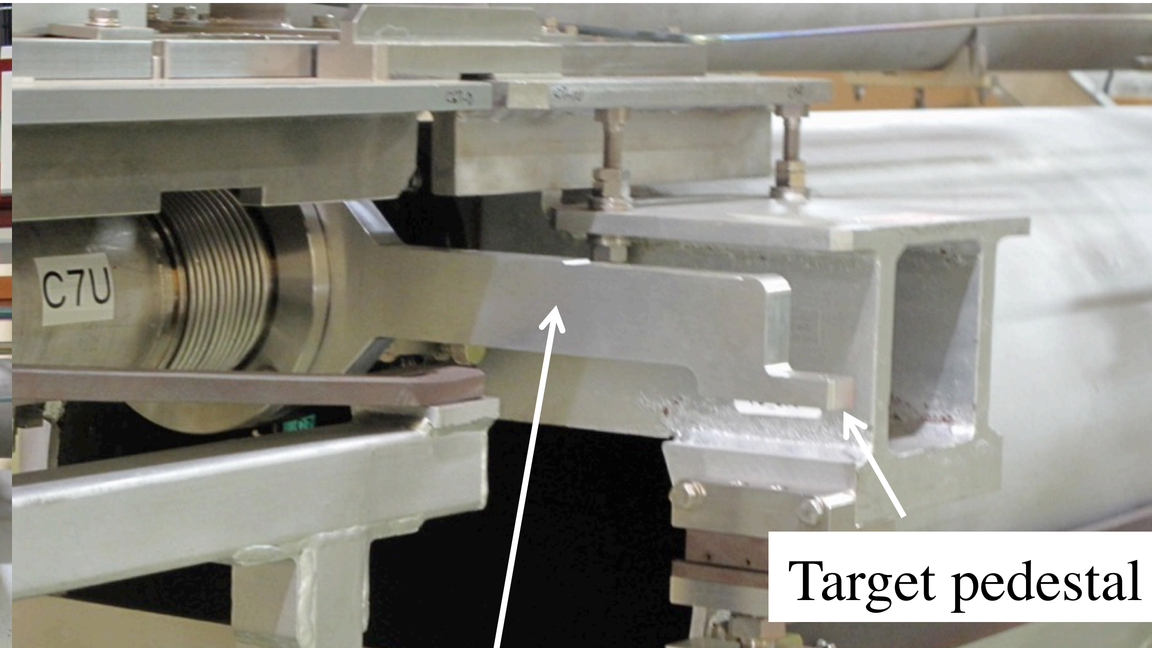

- Special jig (mechanical arm) for fiducialization of a tracker target.
- The jig and QPD are accurately connected by flange-flange mechanical jointing.

Component alignment on the girder

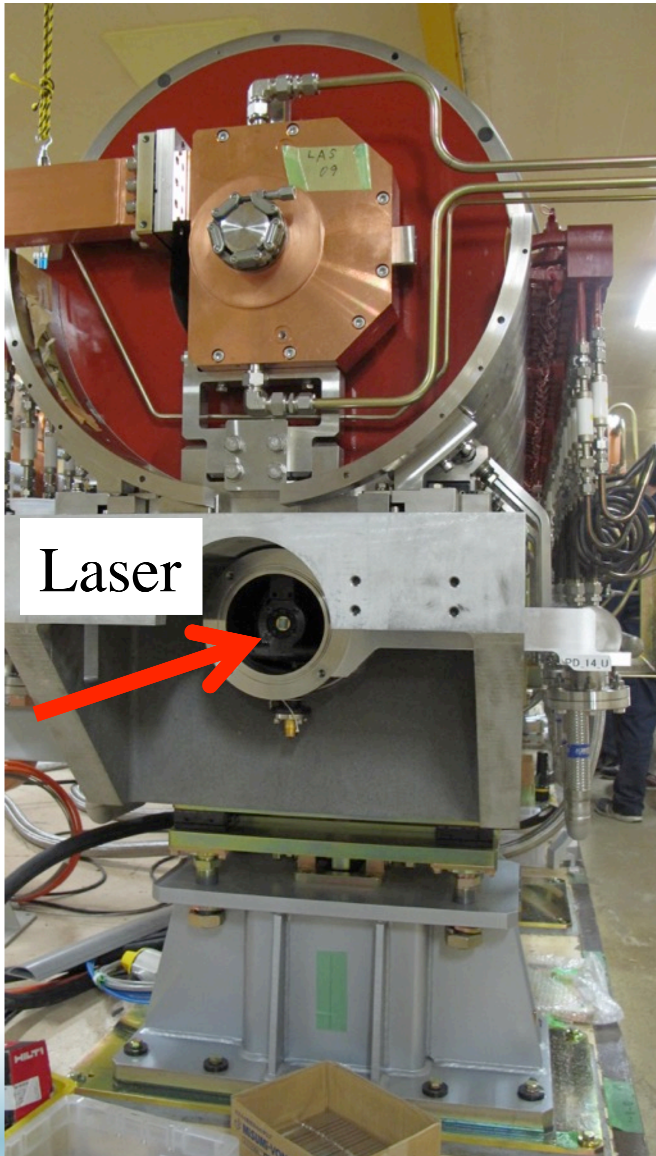

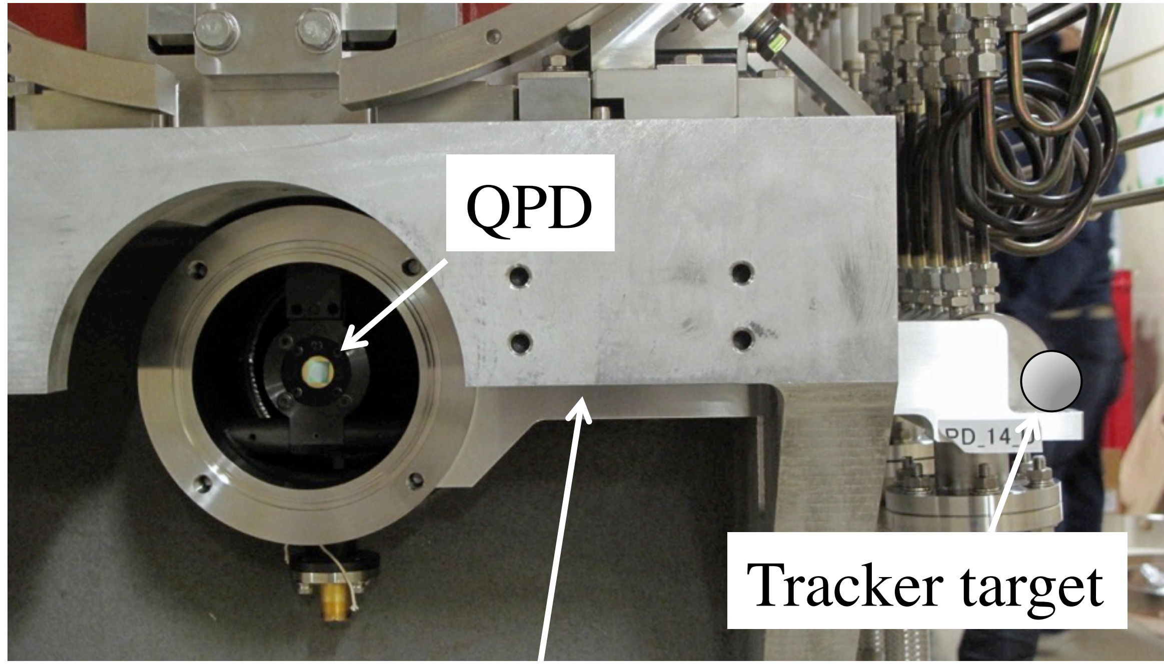

Special jig for fiducialization of tracker target

Isolated floor structure at the optical ystem

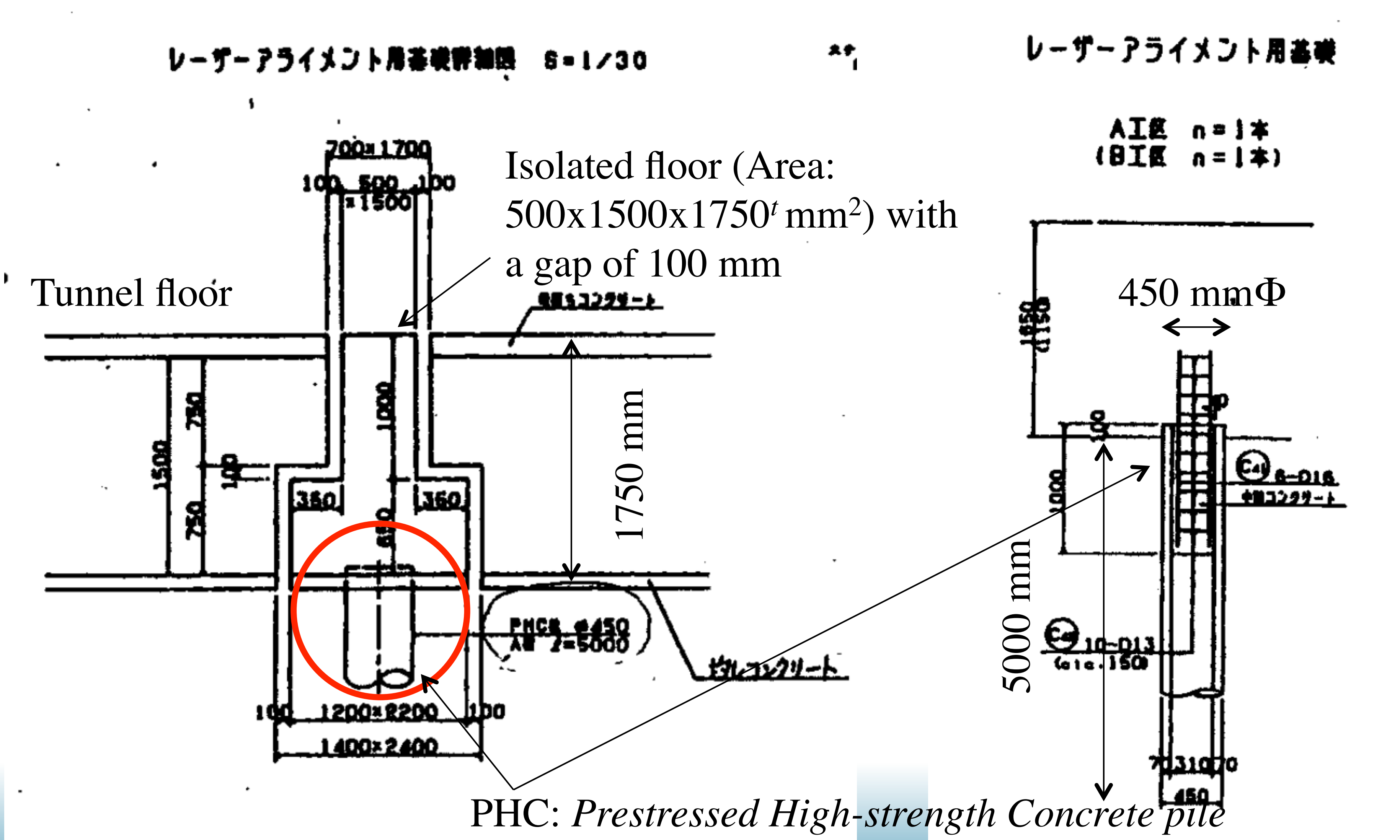

Mechanical jig for fiducialization of tracker target

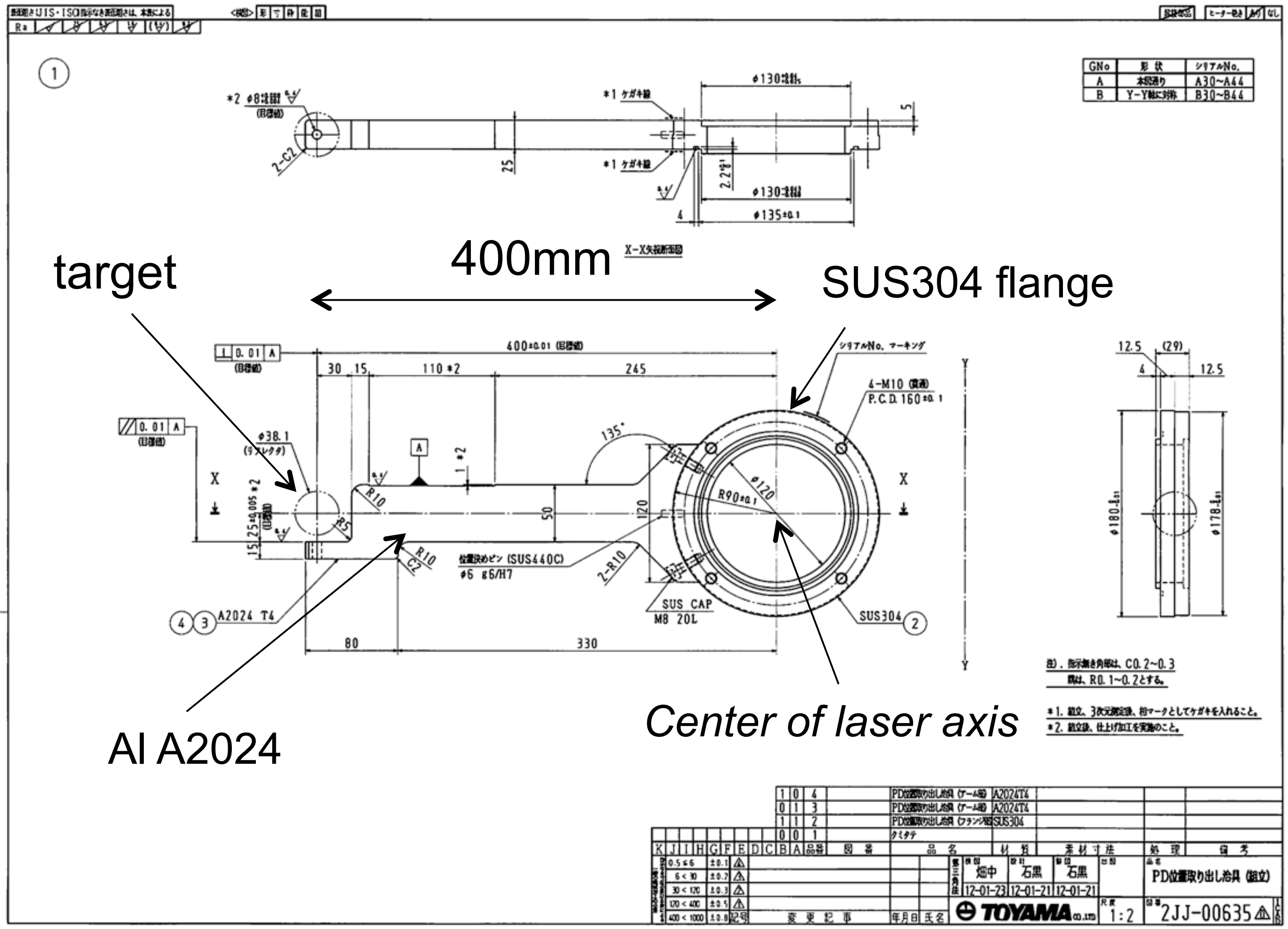

Laser pipe with a viewing port

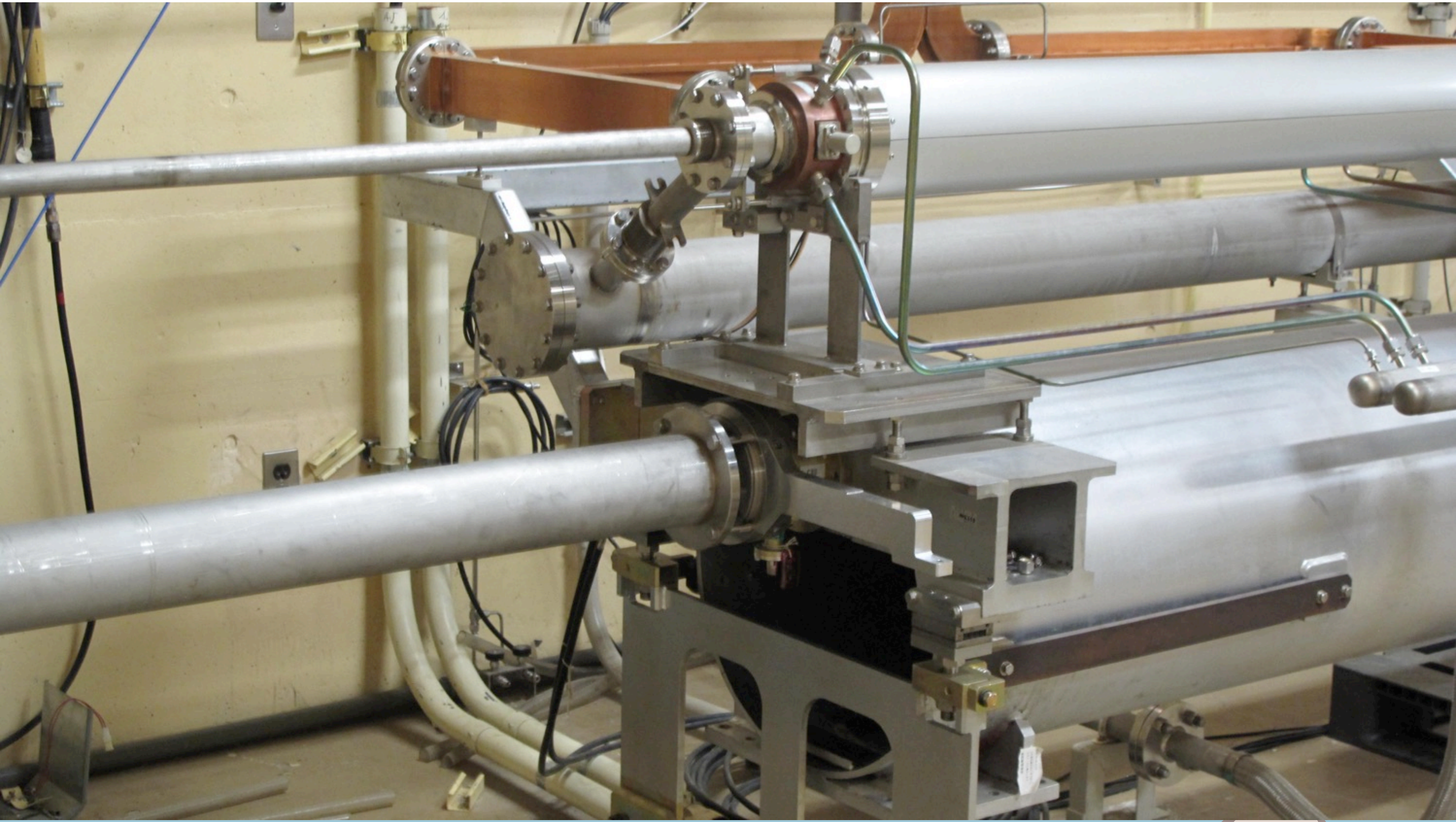

Support of accelerating structures

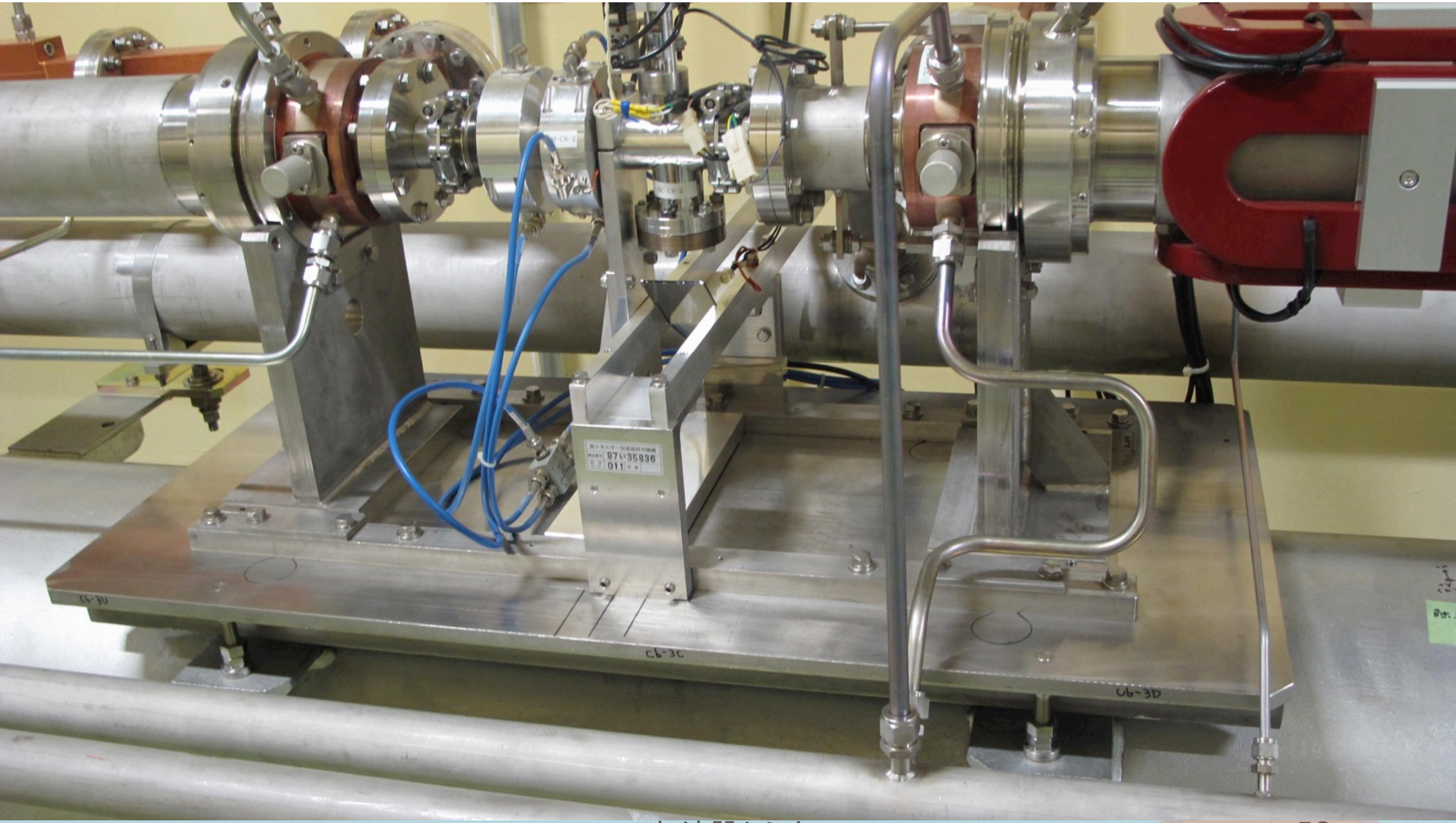

Connection between accelerating structure and Quad

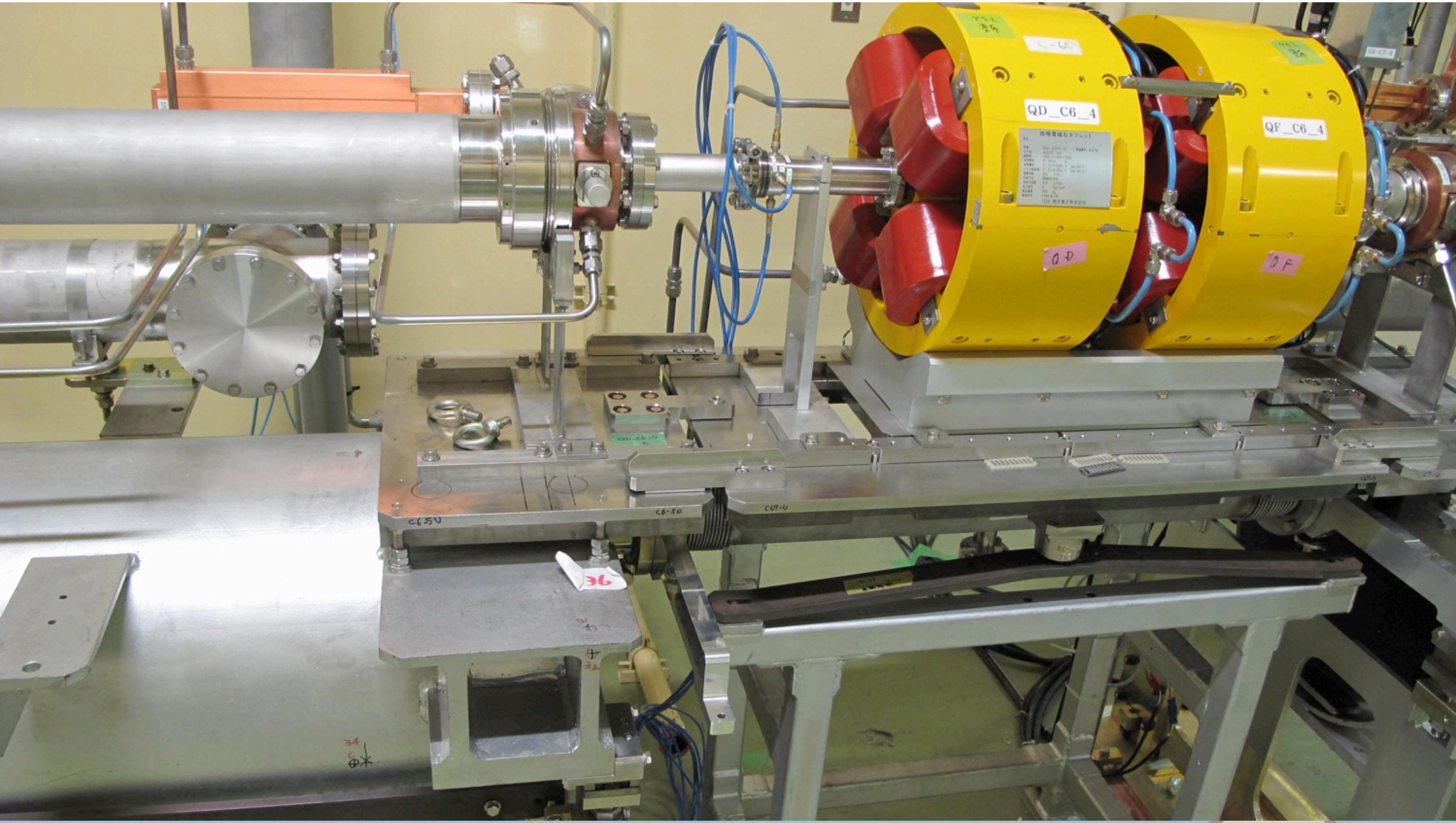

3D mechanical precision measurement in QPD holder

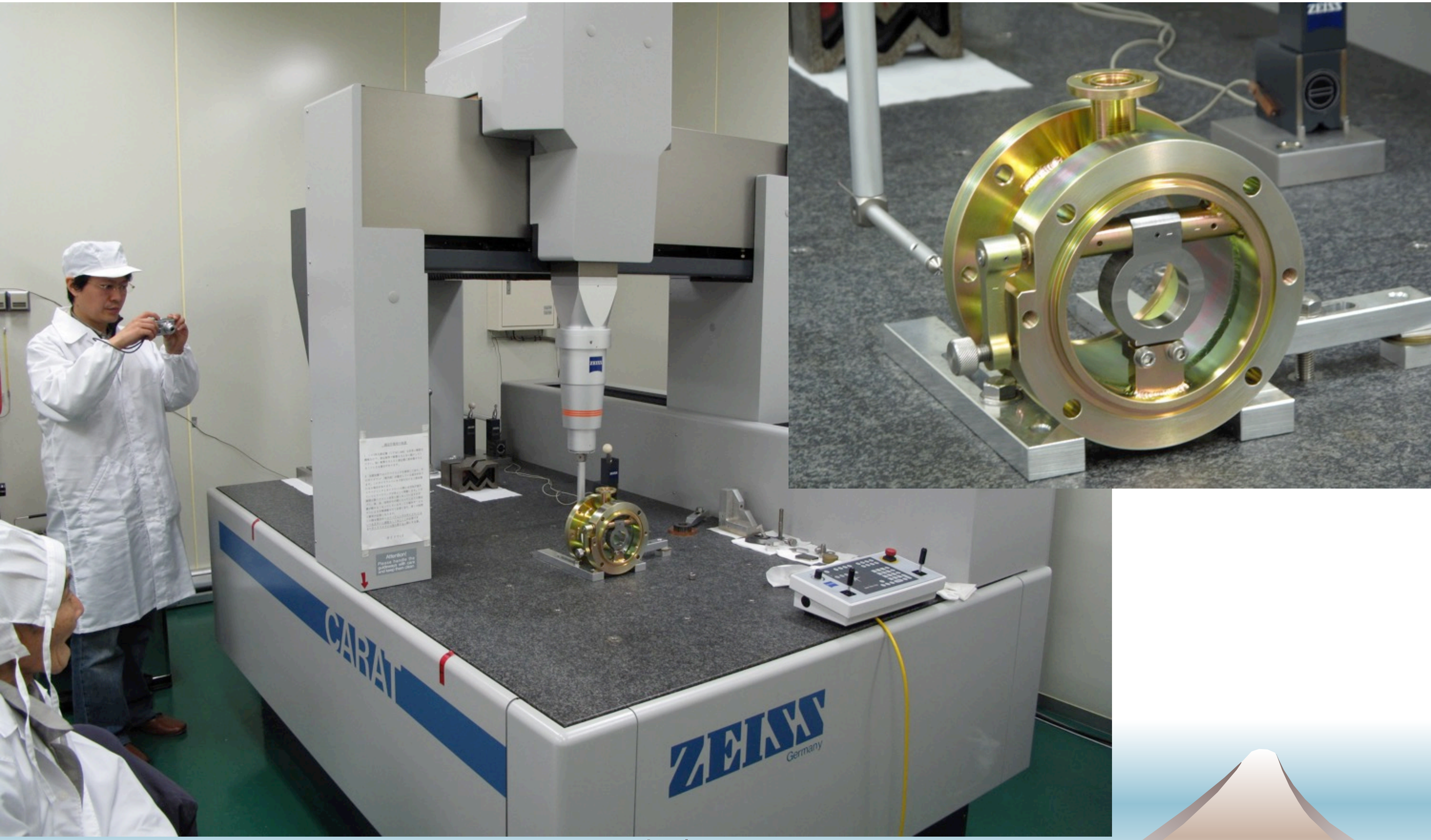

Test bench in QPD setting calibration

Reinforced girder

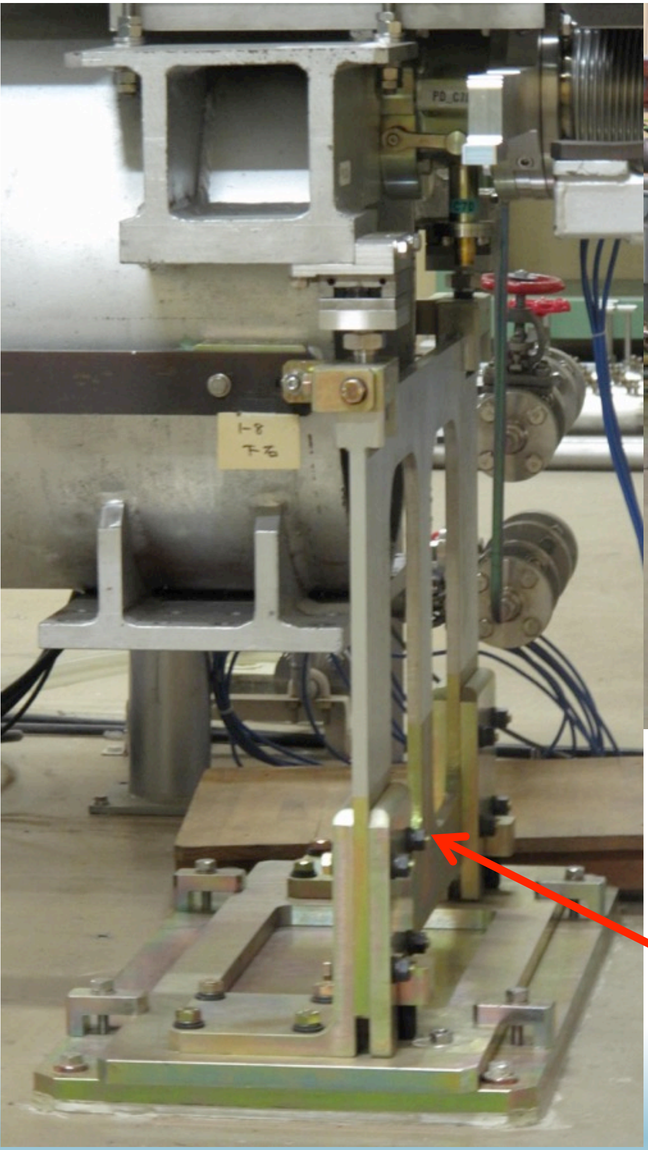

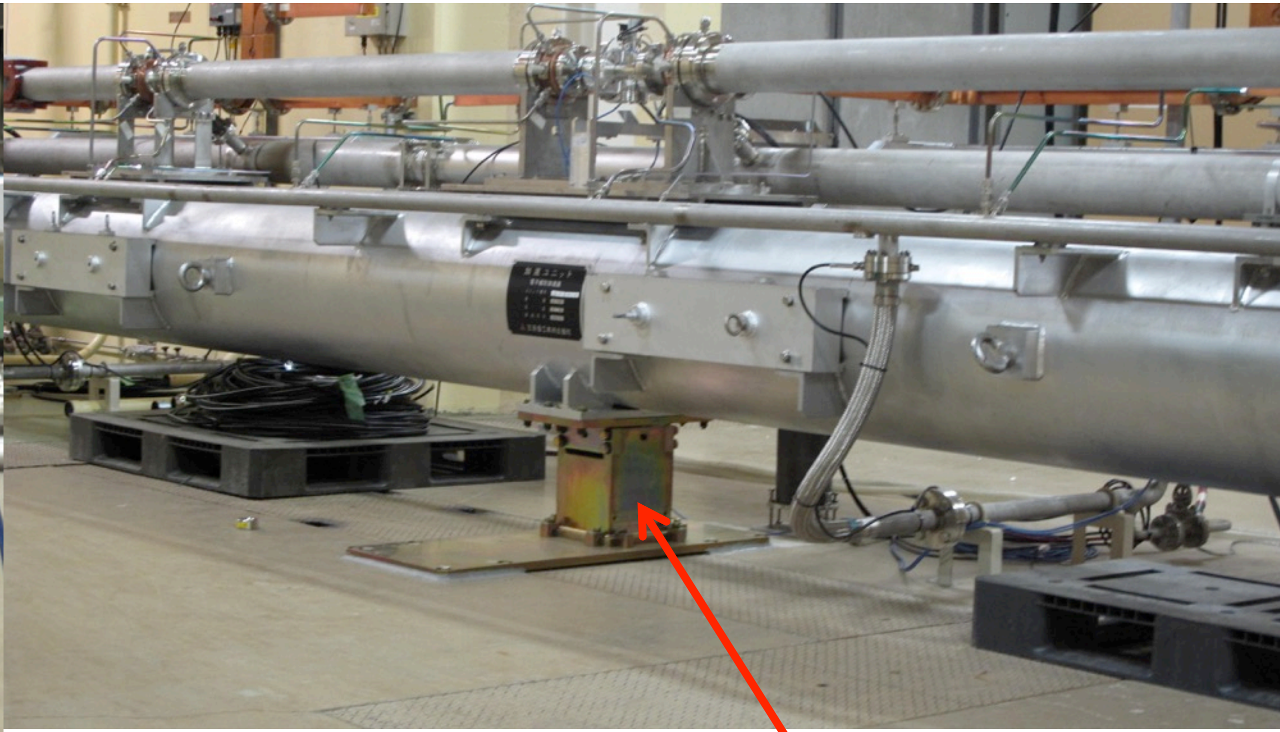

Center support added

Leg reinforced

Ultrafine stage to stabilize the laser pointing

Developments for the laser-based alignment system

- Our laser-based alignment system was first implemented at the construction stage in 1982; however, the high stabilization of the laser-based fiducial line has not been realized until now.
- At long last, a laser line with high stabilization has been implemented as a 500-m-long fiducial line for alignments in March 2013.
- We experimentally investigated the propagation and stability characteristics of the laser line passing through metallic pipes in vacuum.
- Pointing stability at the last fiducial point with the transverse displacements of ±40 μm level in one standard deviation by applying a feedback control was successfully obtained. This pointing stability corresponds to an angle of ±0.08 μrad. This system is now fully exhibiting the successful results for the high-precision alignment of the injector linac currently in progress.

Stability measurements of the laser axes at z=500 m

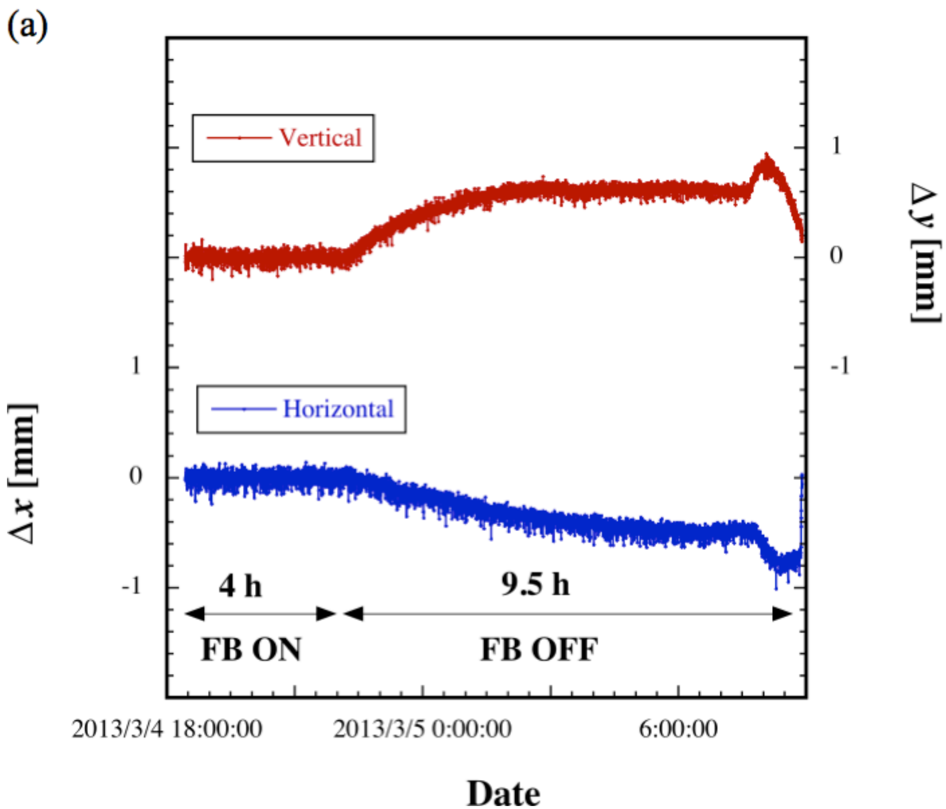

Time traces of the horizontal and vertical position displacements of the laser beam at the last QPD (a) with the feedback control on and off during 13.5 h

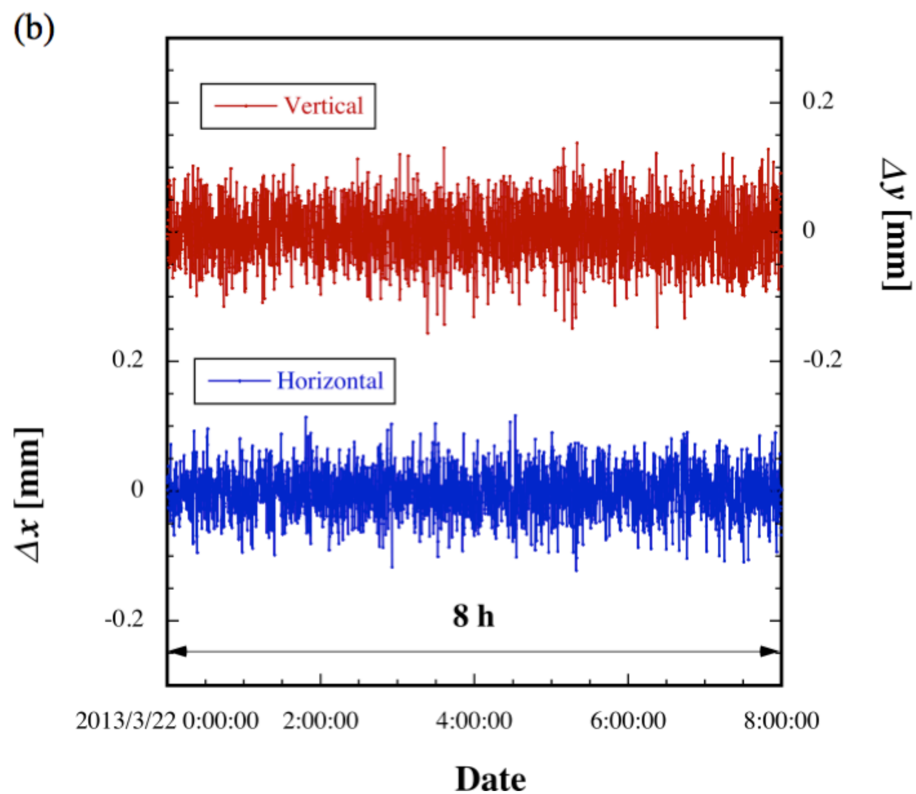

Time traces of the horizontal and vertical position displacements of the laser beam at the last QPD (b) with the feedback control on during 8 h.

Position displacement distribution of the laser axes for 132-m-long straight line

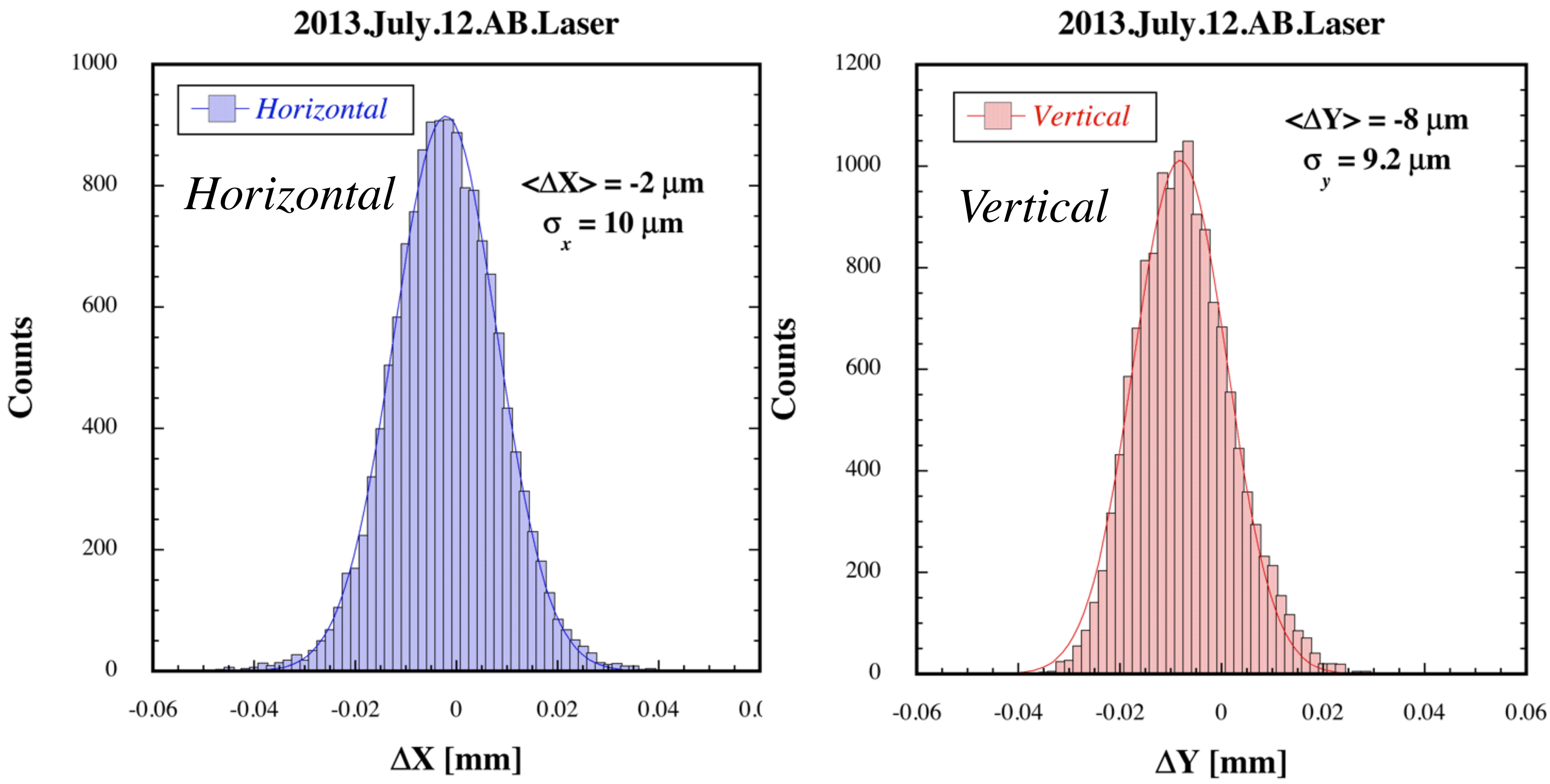

Girder unit for accelerating structures

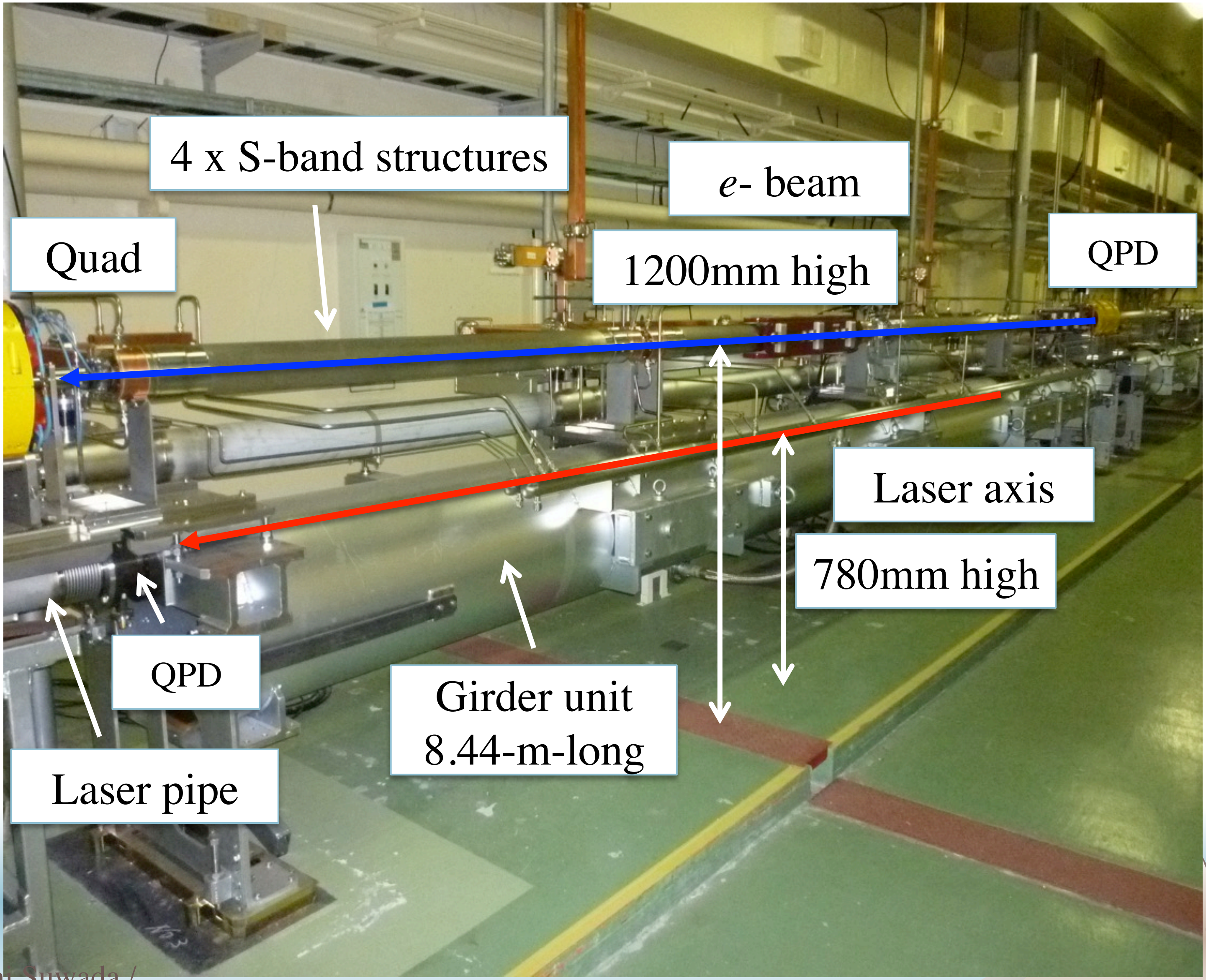

Introduction of the Displacement vectors

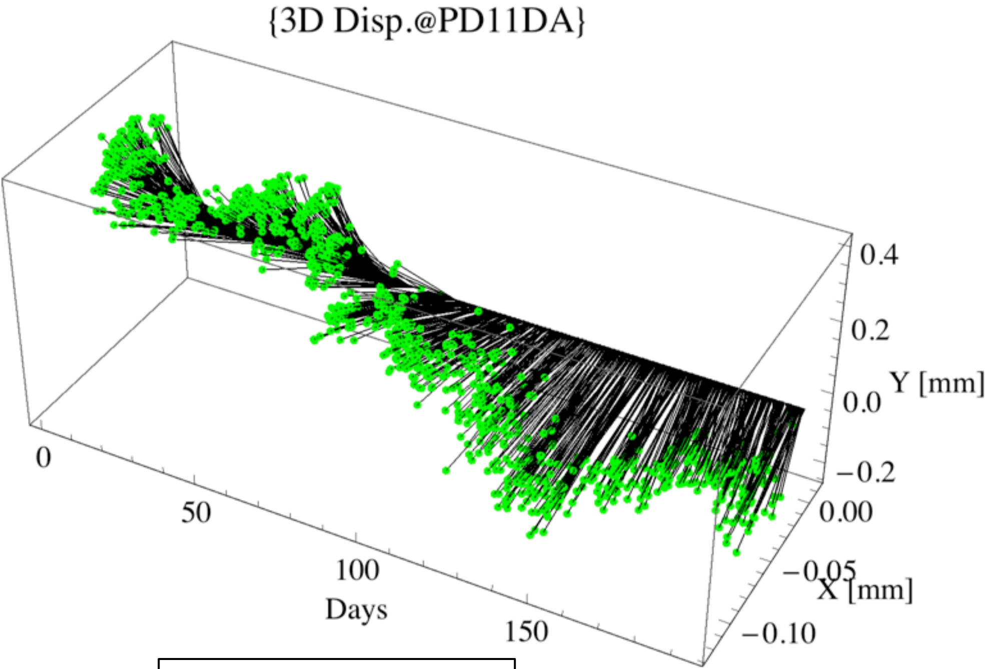

QPD_11DA

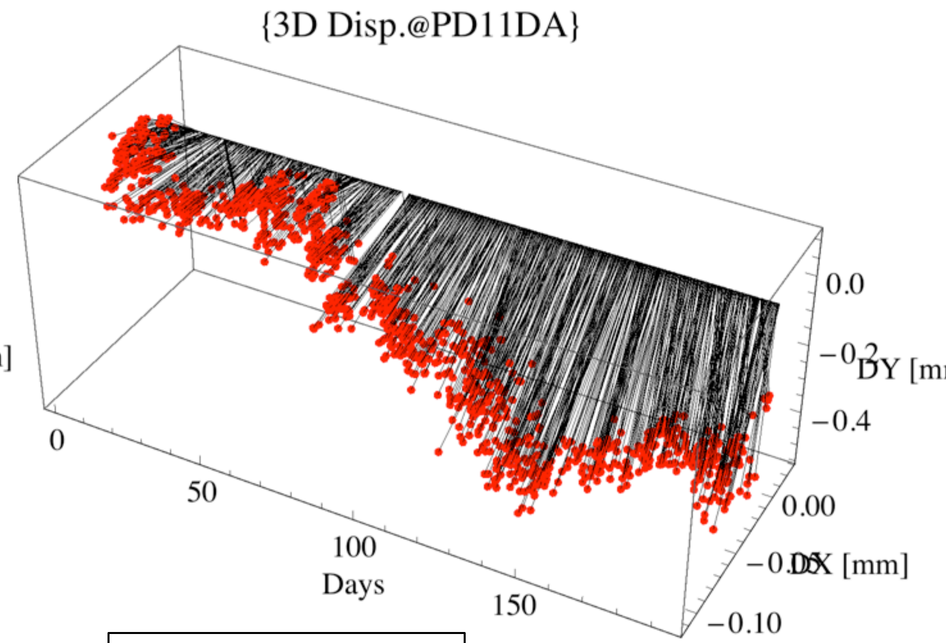

QPD_11DA

- Variations in a time trace of the displacement vector obtained for the accelerator units with the feedback control on.
- It can be seen that the displacement vector has complicatedly rotated around the laser axis along with the growth of the vector norm in the time direction.

Typical displacement vectors @ QPD-38DA

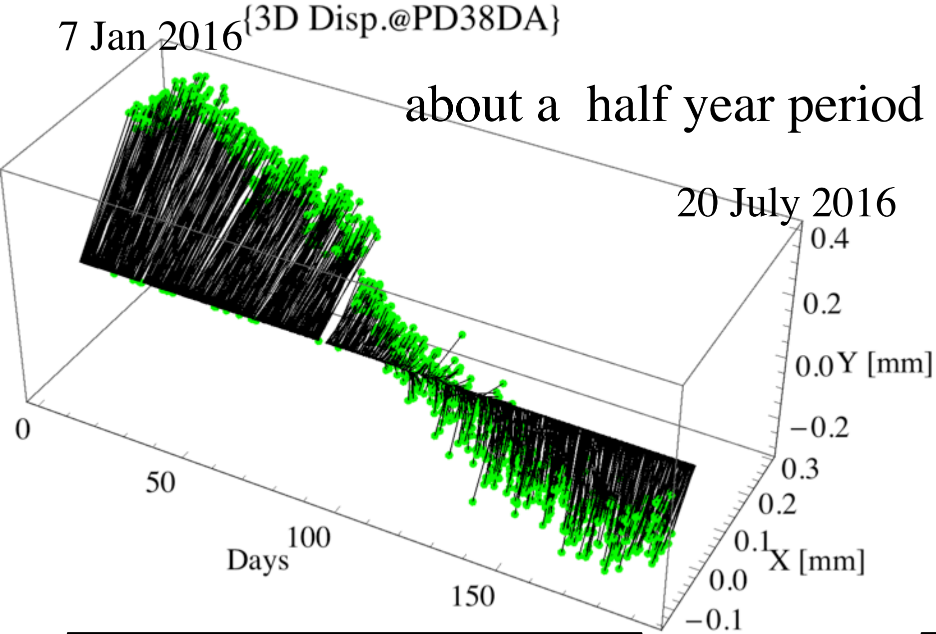

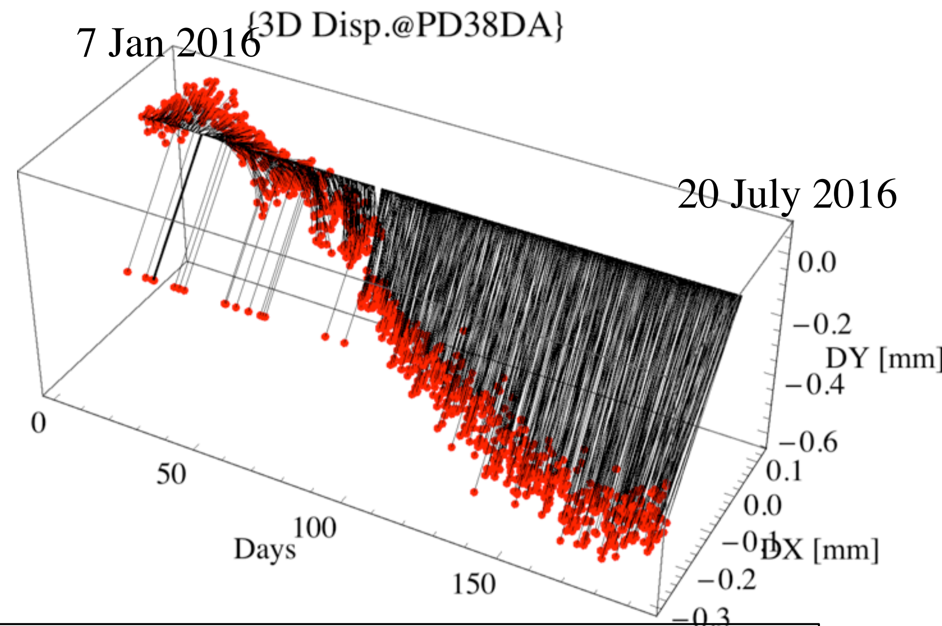

displacement vector

differential displacement vector

- Every four hours on the hour, the basic functions provided by the server start to work in order to take a series of the displacement data for all the QPDs.
- The results show typical variations in a time trace of the displacement vector obtained for the accelerator units with the feedback control on.
- It can be seen that the displacement vector has complicatedly rotated around the laser axis along with the growth of the vector norm in the time direction.

Introduction of the Displacement vectors (cont'd)

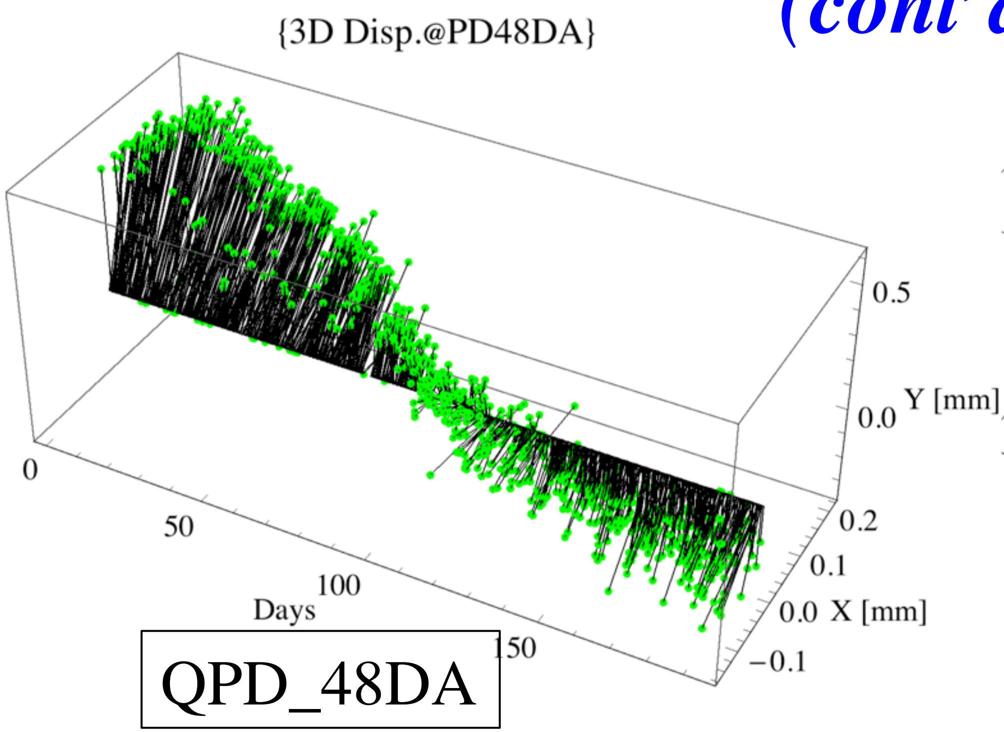

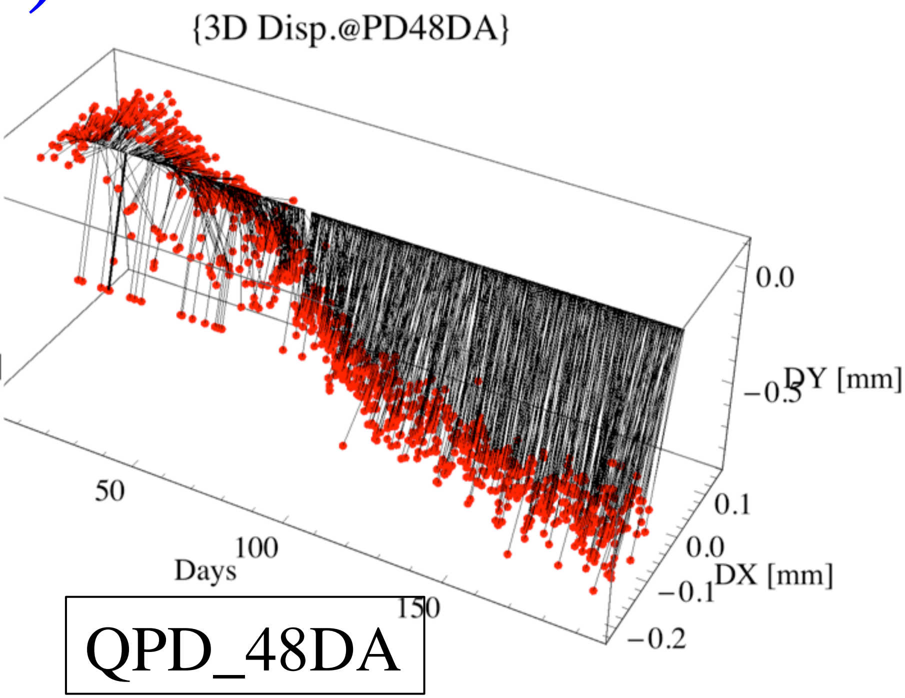

- Variations in a time trace of the differential displacement vector obtained for the accelerator units with the feedback control on.
- It can be seen that the displacement vector has complicatedly rotated around the laser axis along with the growth of the vector norm in the time direction.